The eruption of 22 April 2021 as observed by SolarOrbiter, STEREO and Earth bound instruments

L. Rodriguez (✉ luciano.rodriguez@observatory.be)

Royal Observatory of Belgium

A. Warmuth

Leibniz Institute for Astrophysics Potsdam

V. Andretta

Astronomical Observatory of Capodimonte

M. Mierla

Royal Observatory of Belgium

A. N. Zhukov

Royal Observatory of Belgium

D. Shukhobodskaia

Royal Observatory of Belgium

A. Niemela

KU Leuven

Maharana A.

KU Leuven

M. J. West

Southwest Research Institute

E. K. J. Kilpua

University of Helsinki

C. Möstl

Austrian Academy of Sciences

E. D'Huys

Royal Observatory of Belgium

A. M. Veronig

University of Graz

F. Auchère

University of Paris-Saclay

A. F. Battaglia

University of Applied Sciences and Arts Northwestern Switzerland

F. Benvenuto

University of Genoa

D. Berghmans

Royal Observatory of Belgium

E. C. M. Dickson

University of Graz

M. Dominique

Royal Observatory of Belgium

S. Gissot

Royal Observatory of Belgium

L. A. Hayes

European Space Research and Technology Centre

T. Katsiyannis

Royal Observatory of Belgium

E. Kraaikamp

Royal Observatory of Belgium

F. Landini

Osservatorio Astrofisico di Torino

J. Magdalenic

Royal Observatory of Belgium

G. Mann

Leibniz Institute for Astrophysics Potsdam

P. Massa

University of Genoa

B. Nicula

Royal Observatory of Belgium

M. Piana

University of Genoa

O. Podladchikova

Leibniz Institute for Astrophysics Potsdam

C. Sasso

Astronomical Observatory of Capodimonte

F. Schuller

Leibniz Institute for Astrophysics Potsdam

K. Stegen

Royal Observatory of Belgium

R. Susino

Osservatorio Astrofisico di Torino

M. Uslenghi

Istituto di Astrofisica Spaziale e Fisica Cosmica di Milano

C. Verbeeck

Royal Observatory of Belgium

Research Article

The eruption of 22 April 2021 as observed by Solar Orbiter, STEREO and Earth bound instruments

Solar Physics

L. Rodriguez[1] · A. Warmuth[2] ·
V. Andretta[3] · M. Mierla[1,4] ·
A. N. Zhukov[1,5] · D. Shukhobodskaia[1] ·
A. Niemela[6,1] · A. Maharana[6,1] · M.
J. West[7] · E. K. J. Kilpua[8] ·
C. Möstl[9] · E. D'Huys[1] ·
A.M. Veronig[10] · F. Auchère[11] · A.
F. Battaglia[12,13] · F. Benvenuto[14] ·
D. Berghmans[1] · E. C. M. Dickson[10] ·
M. Dominique[1] · S. Gissot[1] · L.
A. Hayes[15] · T. Katsiyannis[1] ·
E. Kraaikamp[1] · F. Landini[16] ·
J. Magdalenić[1,6] · G. Mann[2] · P. Massa[14] ·
B. Nicula[1] · M. Piana[14] ·
O. Podladchikova[2] · C. Sasso[3] ·
F. Schuller[2] · K. Stegen[1] · R. Susino[16] ·
M. Uslenghi[17] · C. Verbeeck[1]

✉ L. Rodriguez
luciano.rodriguez@observatory.be

[1]   Solar-Terrestrial Centre of Excellence – SIDC, Royal Observatory of Belgium; Avenue Circulaire 3, 1180 Brussels, Belgium

[2]   Leibniz Institute for Astrophysics Potsdam (AIP), An der Sternwarte 16, 14482 Potsdam, Germany

[3]   INAF - Osservatorio Astronomico di Capodimonte, Salita Moiariello 16, I-80131 Naples, Italy

[4]   Institute of Geodynamics of the Romanian Academy, 020032 Bucharest-37, Romania

[5]   Skobeltsyn Institute of Nuclear Physics, Moscow State University, 119992 Moscow, Russia

[6]   CmPA/Department of Mathematics, KU Leuven, Celestijnenlaan 200 B, 3001 Leuven, Belgium

Abstract The Extreme Ultraviolet Imager (EUI) onboard Solar Orbiter observed an eruption through both of its channels (17.4/30.4 nm) of its Full Sun Imager, on 22 April 2021. At the time, the spacecraft was at 0.87 au from the Sun, and 98° east of the Sun-Earth line. The eruption was slightly back-sided, emerging close to the southwest limb, starting at 04:24 UT, with the source located at S20W103 from the Solar Orbiter perspective. The Solar Orbiter coronagraph, Metis, observed the CME at 06:05 UT. The Spectrometer/Telescope for Imaging X-rays (STIX) on Solar Orbiter sampled the associated X-ray flare, which was partially occulted. This allowed the characterization of both the thermal plasma and any potential contribution of non-thermal electrons in the tenuous coronal source. The X-ray source location is compared to the extreme ultraviolet coronal structures seen by EUI, and it is established that STIX imager only sees the top part of the flaring loops, while most of the flare – in particular the non-thermal foot points – remain occulted.

From the Earth's perspective the eruption source region was observed at S20W05 (close to disk centre), the Atmospheric Imaging Assembly (AIA), onboard the Solar Dynamics Observatory (SDO) and the Sun Watcher using Active Pixel System detector and Image Processing (SWAP), onboard the PRoject for Onboard Autonomy (PROBA2) observed dimmings and an associated large-scale coronal wave starting around 04:07 UT. The Extreme Ultraviolet Imager (EUVI) on the Solar-TErrestial RElations Observatory (STEREO-A), located 53° east of the Sun-Earth line at the time, observed similar signatures of an eruption starting around 04:17 UT, on-disk at S20W50. The corresponding CME was observed as a partial halo CME shortly after (∼06:00 UT) by the C2 Large Angle and Spectrometric Coronagraph (LASCO), from the Earth perspective onboard the

7   Southwest Research Institute, 1050 Walnut Street, Suite 300, Boulder, CO 80302, USA

8   Department of Physics, University of Helsinki, PO Box 64, 00014, Helsinki, Finland

9   Space Research Institute, Austrian Academy of Sciences, 8042 Graz, Austria

10   University of Graz, Institute of Physics, Universitätsplatz 5, 8010 Graz, Austria

11   Université Paris-Saclay, CNRS, Institut d'Astrophysique Spatiale, 91405 Orsay, France

12   Institute for Data Science (I4DS), University of Applied Sciences and Arts Northwestern Switzerland, Bahnhofstrasse 6, 5210 Windisch, Switzerland

13   Institute for Particle Physics and Astrophysics (IPA), Swiss Federal Institute of Technology in Zurich (ETHZ), Wolfgang-Pauli-Strasse 27, 8039 Zurich, Switzerland

14   MIDA, Dipartimento di Matematica, Università degli Studi di Genova, Via Dodecaneso 35, 16146 Genova, Italy

15   European Space Agency (ESA), European Space Research and Technology Centre (ESTEC), Keplerlaan 1, 2201 AZ Noordwijk, The Netherlands

16   INAF - Osservatorio Astrofisico di Torino, Via Osservatorio 20, I-10125, Pino Torinese, Italy

17   INAF - Institute of Space Astrophysics and Cosmic Physics of Milano, Italy

SOlar and Heliospheric Observatory (SOHO), and by the STEREO-A/COR2 coronagraph as a clear structured CME around 05:23 UT.

The corresponding ICME arrived at Earth on 24 April 2021, it was driving a shock and created minor geomagnetic storm conditions. We simulate the CME with the 3D MHD heliospheric model EUHFORIA. We provide an analysis of the eruption as observed by these various instruments from different vantage points. The combination of data from Solar Orbiter as well as other space-based assets with numerical modeling clearly showcases the scientific potential for the science phase of Solar Orbiter, and the unique observations available.

Keywords: Coronal Mass Ejections, Low Coronal Signatures; Coronal Mass Ejections, Initiation and Propagation; Prominences, Dynamics

1. Introduction

Coronal Mass ejections (CMEs) are among the most important transient events in the solar system. They comprise huge amounts of plasma and magnetic fields expelled from the Sun, with velocities typically in a range of 400 to 1000 km s^{-1} but these can also be higher than 2000 km s^{-1} (Hundhausen, Burkepile, and St. Cyr, 1994; Dryer *et al.*, 2012; Liou *et al.*, 2014), they can arrive to the Earth within 1-4 days. Upon arrival, its interaction with the Earth's magnetosphere can produce geomagnetic storms, depending on its internal magnetic field and plasma configuration (e.g. Schwenn, 2006; Temmer, 2021; Kilpua *et al.*, 2017; Koskinen *et al.*, 2017). When CMEs are detected in situ by a spacecraft, they are termed Interplanetary CMEs (ICMEs) (e.g. Rodriguez *et al.*, 2011; Kilpua, Koskinen, and Pulkkinen, 2017a), and are recognized by a set of signatures observed in the plasma and magnetic field data (Zurbuchen and Richardson, 2006). CMEs are often connected to flares and accompanied by magnetic energy release and acceleration of electrons and ions, that produce electromagnetic radiation across a broad spectral range, from X-rays to radio waves, making observations with remote-sensing instruments possible (e.g., Fletcher *et al.*, 2011; Benz, 2017). When a CME propagates towards, or away, from the observer it is observed in white-light coronagraph images as *halos* around the occulter, and are therefore called halo CMEs. From the Earth's perspective, such observations indicate eruptions that may be travelling along, or close to, the Sun-Earth line (if front sided), and as such, these ejections have significant importance for space weather (Howard *et al.*, 1982; Schwenn, 2006; Rodriguez *et al.*, 2009). These detections were done mostly made by the SOlar and Heliospheric Observatory (SOHO; Domingo, Fleck, and Poland, 1995, located at the L1 Lagrangian point of the Sun-Earth system) using the Large Angle and Spectroscopic COronagraph (LASCO; Brueckner *et al.*, 1995) to detect CMEs, and complementary EUV observations, such as those made by the Extreme-ultraviolet Imaging Telescope (EIT; Delaboudinière *et al.*, 1995), to detect the associated signatures in the low corona, like coronal dimmings, "EIT waves", post-eruption arcades, erupting filaments (e.g. Zhukov, 2007). However that was changed with the launch of the Solar-TErrestial RElations Observatory (STEREO; Kaiser *et al.*, 2008), which

provided a view from a location away from the Sun-Earth line using the COR coronagraphs and the Extreme Ultraviolet Imagers (EUVI) of the Sun Earth Connection Coronal and Heliospheric Investigation instrument suites (SECCHI; Howard *et al.*, 2008).

When STEREO was positioned away from the Sun-Earth line, especially when it was near quadrature positions, it allowed the tracking of Earth-directed CMEs from a side view (e.g. Davies *et al.*, 2009; Möstl *et al.*, 2011; Rodriguez *et al.*, 2020). The placement of spacecraft away from the Sun-Earth line provides a crucial viewpoint needed for an early characterization of Earth-directed CMEs, in particular for determining the CME propagation direction, speed and acceleration.

In 2010, the Solar Dynamics Observatory (SDO; Pesnell, Thompson, and Chamberlin, 2012) was launched. It became an important tool in CME studies, in particular its Atmospheric Imaging Assembly (AIA; Lemen *et al.*, 2012) instrument, which provides high-cadence and high-resolution images of the solar corona through EUV passbands, allowing further characterization of lower coronal signatures. The PRoject for Onboard Autonomy (PROBA2) satellite (Santandrea *et al.*, 2013) also started its scientific mission in 2010 (launched in 2009), carrying the Sun Watcher with Active Pixels and Image Processing (SWAP; Seaton *et al.*, 2013; Halain *et al.*, 2013) imager. This single passband (centred on 17.4 nm, around the Fe IX/X emission lines, corresponding to a plasma temperature of log T $\approx$ 6.0 K) large field-of-view imager (FOV; 54$\times$54 arcmin; 1.8 Rs$\times$1.8 Rs), 1024$\times$1024 pixel (3.2 arcsec pixels). SWAP provides the widest EUV observations of the Sun from the Earth perspective, extending into the middle corona, and allows further characterisation of eruptions occurring near the solar limb, especially during their impulsive phase.

More recently, in 2020, Solar Orbiter (SolO; Müller *et al.*, 2020) was launched. Even though it is not a mission dedicated to space weather monitoring, this spacecraft provides an important perspective into the study of CMEs, with its eccentric orbit that will bring it as close as 0.28 au to the Sun, as well as reaching inclinations of 33° from the solar equator. In this paper, we showcase how SolO instruments can be used to observe a CME and and associated flare in detail, analyse them, and model the CME propagation all the way to the Earth.

The remote sensing instruments onboard SolO, used in this study include: the Extreme Ultraviolet Imager (EUI; Rochus *et al.*, 2020) which provides high-resolution images of the lower corona through three EUV passbands; the Metis coronagraph (Antonucci *et al.*, 2020), which allows the observation of the heliosphere, and CMEs, in the visible light and in ultraviolet; and the Spectrometer/Telescope for Imaging X-rays (STIX; Krucker *et al.*, 2020), which provides information on high energy flaring activity.

Since its launch in 2020, SolO has observed a number of CME and ICME events. Andretta *et al.* (2021) described the first CME observed by Metis through its visible and UV channels, on 16 January 2021. Möstl *et al.* (2022) reported on the first search for multipoint in-situ and imaging observations of ICMEs in SolO data up to April 2021. Telloni *et al.* (2021) studied the interaction of two CMEs in June 2020. O'Kane *et al.* (2021) reported on a stealth CME (eruptions with difficult to determine lower coronal signatures) sampled by SolO on 19 April

2020. This same CME was observed by Bepi Colombo and the Wind spacecraft, and triggered numerous studies by other authors: Weiss *et al.* (2021) used it to test a flux rope model, Kilpua *et al.* (2021) studied the internal structure of the CME sheath, Zhao *et al.* (2021) analysed turbulence in the vicinity of the shock driven by the CME, Davies *et al.* (2021) used flux rope models to interpret the large-scale structure of the ICME, and Freiherr von Forstner *et al.* (2021) studied a Forbush decrease related to this CME.

The above mentioned SolO instrumentation were used to observe a CME which erupted on 22 April 2021 in detail, when positioned 98° east of the Sun-Earth line. This event was of particular interest from the point of view of the associated flare, as it was partially occulted from the SolO perspective while it was fully visible from the Earth. A combination of STIX and EUI observations allowed us to establish the origin of the emission (Section 3). These observations are described here, together with observations of the arrival of the ICME in situ at the Earth. A simulation of its propagation, performed with a 3D MHD heliospheric model (EUHFORIA; Pomoell and Poedts, 2018), is included to help characterise the eruptions kinematics. To obtain the input parameters needed to run EUHFORIA, we combined data from SOHO/LASCO-C2, STEREO-A/COR2 and SolO/Metis.

The paper is organized as follows. Section 2 presents observations of the CME from SolO (EUI and Metis), Earth (AIA, SWAP, and LASCO) and STEREO (EUVI and COR) perspectives. Section 3 describes the observation and analysis of the flare using SolO/STIX. Then, in Section 4 we show the in situ observations of the corresponding ICME as it arrived to the Earth. We then describe the EUHFORIA simulations of the ICME propagation in Section 5. Finally, conclusions are drawn in Section 6.

2. CME Observations

The positions of the various spacecraft at the time of the eruption are shown in Figure 1. The schematic highlights the direction of propagation, which can be seen directed towards the Earth in heliospheric longitude (albeit to the south of the ecliptic, not shown). From the SolO perspective the CME was a far-side event (with the source region just behind the west limb). In the following subsections we outline the observations from the various instruments.

2.1. SolO/EUI observations

The Extreme Ultraviolet Imager (EUI) onboard SolO consists of three telescopes: the Full Sun Imager (FSI), which observes through two EUV bandpasses (17.4 nm and 30.4 nm); and two High Resolution Imagers (HRIs). One of the HRI telescopes, labelled 'HRIEUV', has a bandpass centred on 17.4 nm. The second HRI telescope, labelled 'HRILya', has a bandpass centred at 121.6 nm and is dominated by the Lyman-α hydrogen line.

On 22 April 2021, when the spacecraft was at 0.87 au from the Sun, EUI was operating through a commissioning phase, and only the FSI telescope was
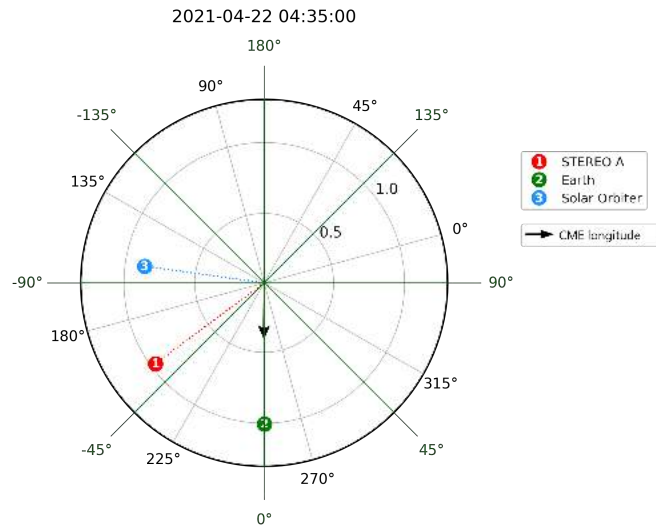
2021-04-22 04:35:00

Figure 1. Positions of the Earth, Solar Orbiter (SolO), and STEREO-A on 22 April 2021. Angles in black are in Carrington coordinates, and angles in green are in the Stonyhurst coordinate system. The figure was created using SOLAR-MACH (https://solar-mach.github.io).

operating. FSI was primarily observing in a synoptic mode, taking images with a cadence of 7.5 minutes with 10 seconds exposure time. The eruption was first observed by EUI at 04:24 UT, through both of its channels (17.4 and 30.4 nm), see Figure 2. The source was located close to the south-west limb, and was partially backsided (S20W103) from the SolO perspective, with the footpoints positioned beyond the limb. Movies are available in the online version of the paper.

Figure 3 shows a sequence of EUI/FSI 17.4 nm images of the early stages of the eruption, where bright magnetic loop structures above the source region are observed to expand significantly in size, showing that the cavity arises coherently through the corona. EUI's exceptional field of view at this time allows the eruption to be tracked in the EUV out into the middle corona. The absence of core dimmings on disk (also visible in the online movies) provides an indication that the source region is at least partially backsided. This will be further demonstrated by the STIX observations (see Section 3).

To analyse the kinematics of the eruption, we tracked the top of the loop at a position angle (PA) of around 245°. The derived heights and speeds versus time are shown in the upper and middle panels of Figure 4 respectively. The speed was calculated by fitting a second order polynomial to the height–time points. We see that the speed is increasing from around 200 km s^{-1} to 450 km s^{-1} when the CME propagated from ~ 1.1 to 2.2 $R_\odot$.

2.2. SolO/Metis observations

The Metis coronagraph onboard SolO provides images of the corona simultaneously in polarised broad-band visible light (VL) in the spectral interval of
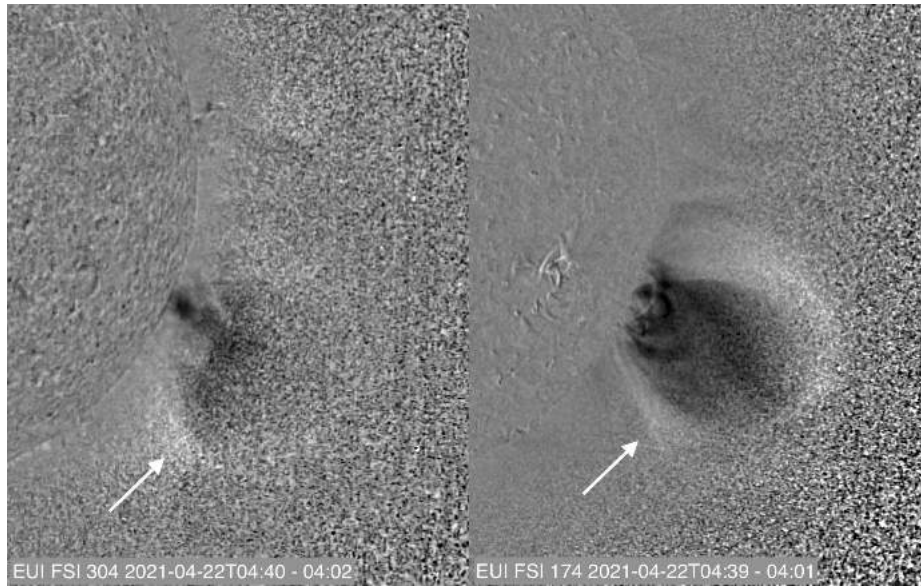
Figure 2. Base difference EUI/FSI observations of the eruption observed on 22 April 2021 at ~04:00 UT through the 30.4nm (left panel) and 17.4nm (right panel) passbands. The white arrows indicate the southern extent of the eruption. Movies are available in the online version.

580-640 nm, and UV narrow-band passband centered around the 121.6 nm H I Ly-α line (Antonucci *et al.*, 2020). The instrument square FOV is $\pm 2.9°$ wide, with an inner circular occulted area of radius $1.6°$. At the time of the observations described in this paper, the instrument FOV covered plane-of-the-sky projected radial distances from 5.2 to 9.4 $R_\odot$, with an unbinned plate scale of $10.14''$/pixel and $20.4''$/pixel in the VL and UV channels respectively.

The eruption was observed while the instrument was performing a test synoptic program; the data set comprises one VL polarized-brightness (pB) sequence and three UV images every hour. The pB sequence consisted of four polarimetric images each acquired with detector integration time of 30 s; the sequence was repeated 15 times, and each set of 15 polarimetric frames was then averaged on board. As a result, each polarimetric image sent to ground – and consequently the corresponding pB image in the data set – was acquired over the course of ~30 minutes. The three UV images were also the result of an on-board average of 15 individual frames, each acquired with detector integration time of 60 s, resulting in a total integration time of ~15 minutes for each image. All images were taken with a 4×4 pixel binning, corresponding to a spatial scale in the plane of the sky (at 0.87 au from the Sun) of ~ 25400 km/pixel for the VL channel and ~ 50000 km/pixel for the UV channel. The acquired data were processed and calibrated following the procedure described in Romoli *et al.* (2021) and subsequently updated as described in Andretta *et al.* (2021).

The CME first appears in Metis images at ~05:30 UT, about 90 minutes after the eruption was first observed by EUI (see Figure 5), at position angles of about $240° – 250°$ (measured anti-clockwise from the north pole). The eruption

EUI FSI 174 2021-04-22T04:31:48.345

EUI FSI 174 2021-04-22T04:39:18.347

EUI FSI 174 2021-04-22T04:46:48.347

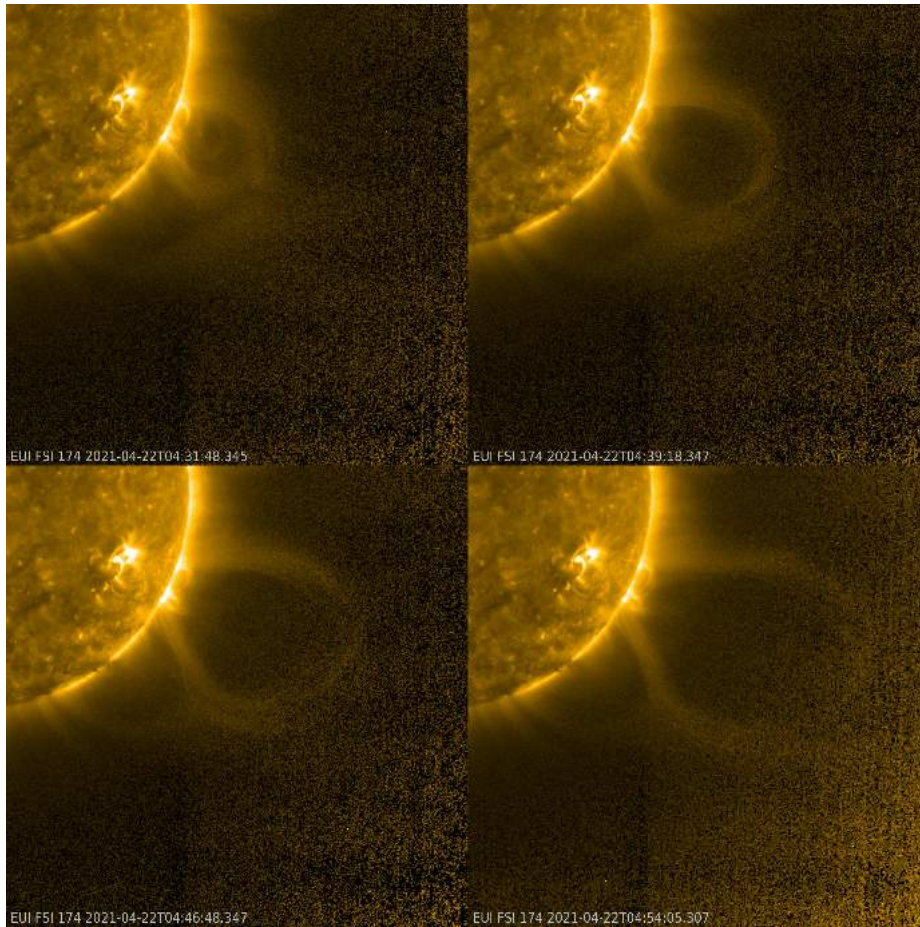EUI FSI 174 2021-04-22T04:54:05.307

Figure 3. Sequence of EUI/FSI 17.4 nm images of the eruption on 22 April 2021.

is observed to emerge to the South of the ecliptic plane, but most likely with a component along the Sun-Earth line, which may arrive to the Earth (see Section 4).

A sequence of images showing the evolution of the eruption as seen in both Metis channels is shown in Figure 6. The eruption front can be seen mainly in the pB images of the second and third panels of Figure 6, trailed by a faint compact feature seen in both channels, marked with an arrow in the figure, perhaps of a similar nature to the blob described in detail by Bemporad *et al.* (2022).

Compared with the events discussed by Andretta *et al.* (2021) and Bemporad *et al.* (2022), the UV (Ly-α) observations seem less structured and display less contrasted features than their pB counterparts. Those events, however, were detected when SolO was situated at a closer distance from the Sun (less than 0.6 au in both cases): it could be speculated that the much reduced Ly-α emission at the larger heliocentric distances observed by Metis in this case could help to
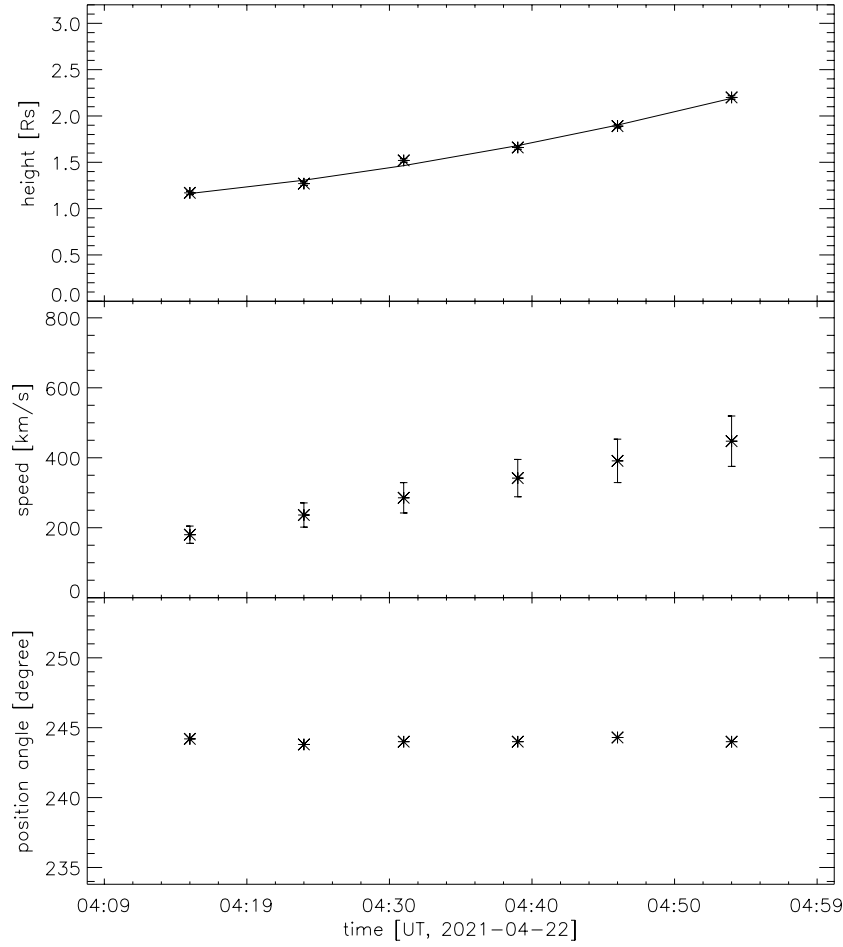
Figure 4. Kinematics of the top of the loop as observed by EUI FSI 174. Upper panel: projected height versus time. The continuous curve shows the second order polynomial fit to the tracked points. Middle panel: Projected speed versus time. Lower panel: Position angle versus time. The errors in the height-time plot correspond to a 5 pixel pointing localisation (which translates to 0.019 Rs).

explain the small contrast of CME features in the UV channel over the background corona. In addition, because of the reduced coronal Ly-α emission, these Metis UV images could even include a contribution by the relatively featureless background interplanetary Ly-α emission (see values in the catalog of UVCS CMEs by Giordano *et al.* 2013 and the average value of the interplanetary Ly-α given by Kohl *et al.* 1997). Finally, the Doppler dimming effect at the estimated speed of this event (Figure 4) would certainly be significant (e.g.: Dolei *et al.*, 2018; Bemporad, Pagano, and Giordano, 2018), thus further contributing to reducing the Ly-α emission.
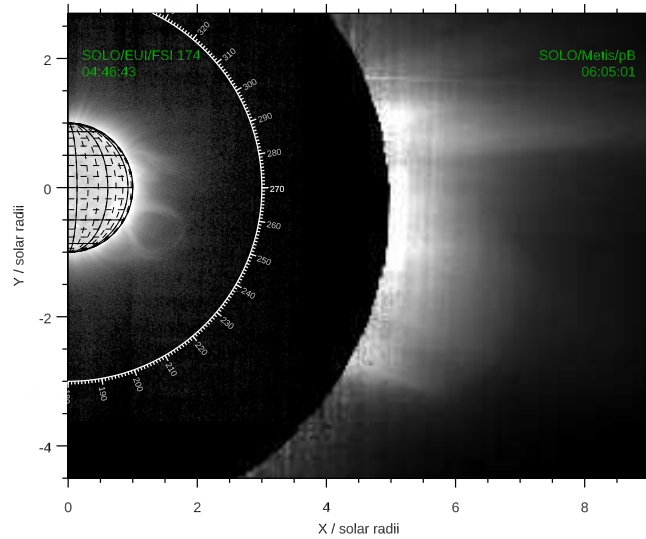
Figure 5. A combined EUI and Metis image of the event. The Metis image was processed with the Normalising Radial Graded Filter (NRGF, Morgan, Habbal, and Woo, 2006), a simple filter often used to remove the strong gradient in coronal intensities and thus reveal coronal structures.

Regarding the kinematics of the event, the Metis data set was not optimized for observing transients: at a one hour cadence, CME features are seen in one or two images only. Moreover, the long integration times may induces a significant blur in moving features, especially during the 30 minutes needed to create a single pB image. It is therefore difficult to give a reliable estimate of the event speed from Metis images. Nevertheless, a simple estimate of the shift of the CME front between the 06:20 and 07:20 pB images of Figure 6 seem to indicate a speed compatible with the values shown in Figure 4.

2.3. The Earth and STEREO perspectives

The eruption was observed through the 17.4 nm EUV bandpass of the SWAP instrument, where the source region was identified near solar disk center, at S20W05, with an associated coronal dimming (Thompson *et al.*, 1998; Dissauer *et al.*, 2018) and "EIT wave" (also called EUV wave; Zhukov, 2011; West *et al.*, 2011; Liu and Ofman, 2014; Warmuth, 2015; Long *et al.*, 2017), see Figure 7 (a). At the time of eruption, SolO was located towards the East of the Sun, from the Earth's perspective (see Figure 1), and the PROBA2 satellite was performing an off-point campaign (pointing to the East) to support EUI observations and image the extended solar corona in that direction. Therefore, the Sun is not centered
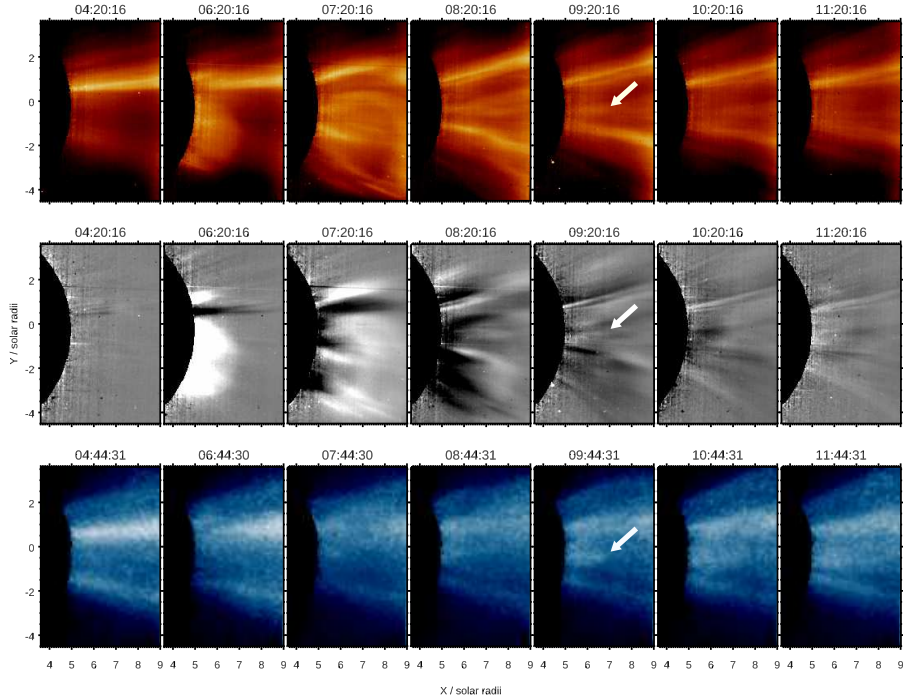
Figure 6. Evolution of the CME as seen by Metis. Top row: pB images, processed with the NRGF algorithm; middle row: pB running difference images; bottom row: UV images processed with the NRGF algorithm. The arrows point to the feature mentioned in the text trailing the CME front.

in the SWAP images. The coronal dimmings associated with the eruption were also observed by AIA, as detected by Solar Demon[1]

In Figure 8, we present AIA observations through the 13.1 nm and 19.3 nm bandpasses, at selected times. The AIA 13.1 nm observations sample the Fe XX–Fe XXIII lines at temperatures greater than 1×10^7 K (top row), and show the eruption of a hot sigmoid (Figure 8, top row), which is generally taken as an indication of a flux rope (e.g., review by Green *et al.*, 2018). The inclination of the erupting sigmoid/flux rope is small, i.e., its main axis is aligned close to the equatorial plane. This is in line with the Graduated Cylindrical Shell (GCS) model (Thernisien, 2011) reconstruction of the associated CME that gave a small tilt of 12° (cf. Table 1 and Figure 9), see below for a more detailed discussion. It is also interesting to note that there are three distinct dimming footpoints associated with the eruption, well seen through the AIA 19.3 nm passband (Figure 8, bottom row). Two are located on the two ends of the hooked flare ribbons, and the third one (which is actually the strongest) is located further remote to the West of the active region at one end of the erupting sigmoid.

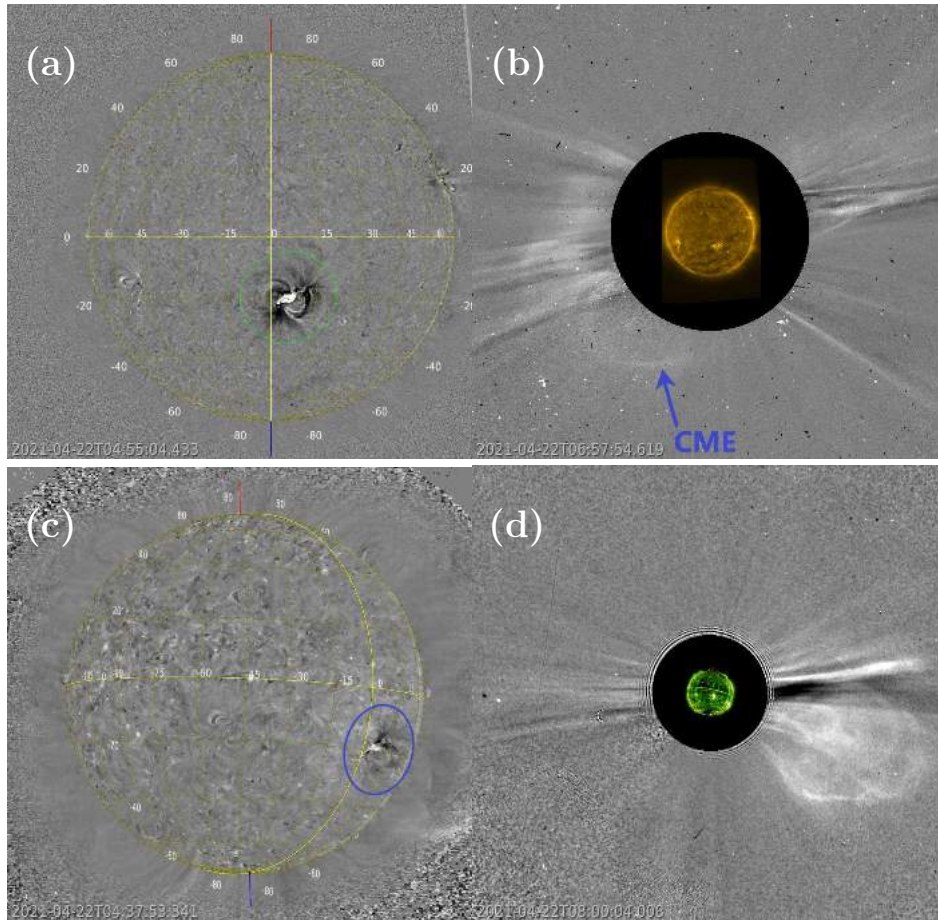[1]https://www.sidc.be/solardemon, see Kraaikamp and Verbeeck (2015).

Figure 7. Observations of the eruption observed on 22 April 2021 from the PROBA2, SOHO, and STEREO-A vantage points. (a) PROBA2/SWAP 17.4 nm running difference image (previous image subtracted) of the associated post-eruptive arcade and coronal dimming (inside the green oval). (b) Running difference image of the CME as seen by SOHO/LASCO-C2 in the southeast, with an SDO/AIA image observed through the 17.1 nm passband overlaid in the centre. (c) STEREO-A/EUVI 19.5 nm running difference image of the eruption showing coronal dimmings (blue circle) near the west limb. (d) STEREO-A/COR2 image of the CME, seen travelling mostly to the west. An image taken by EUVI in the 19.5 nm passband is shown overlaid in the centre. The images were created with JHelioviewer (Müller *et al.*, 2017).

The accompanying CME was observed by LASCO as a faint partial halo directed towards the southeast (Figure 7 (b)). It had an angular width of around 130° and a plane-of-the-sky projected speed of 308 km s^{-1} as measured by the CACTus automated CME detection software [2], see Robbrecht and Berghmans (2004).

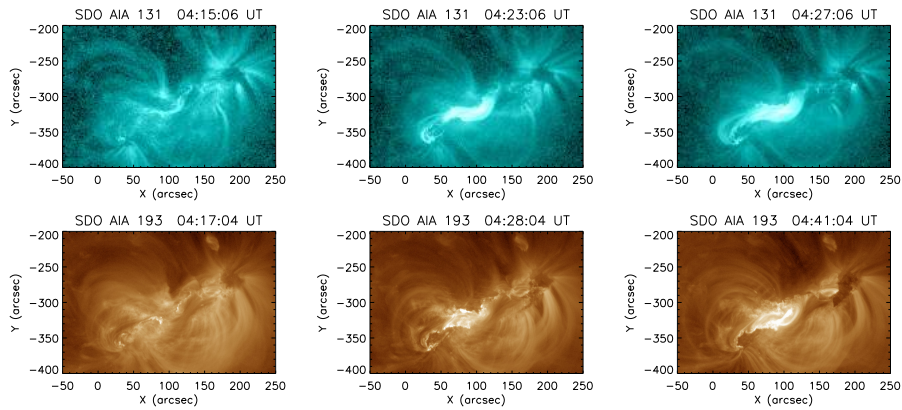---

[2]https://wwwbis.sidc.be/cactus/

Figure 8. SDO/AIA observations of the 22 April 2021 event. The top panels show a sequence of AIA 13.1 nm images highlighting the erupting sigmoid and the flaring arcade. The bottom panels show AIA 19.3 nm images featuring the coronal dimming and flare ribbons.

STEREO-A was located 53° to the east of the Earth (see Figure 1), which allowed observations of the CME and propagation close to the limb, as opposed to the centered view from the SOHO, PROBA2, and SDO perspective. Figure 7 (c) shows the CME source region through the EUVI 19.5 nm EUV passband. The eruption can be identified emerging to the south west, together with an EIT wave propagating along the limb and across the disk and coronal dimmings located at the source region. Figure 7 (d) shows the CME as it emerges out through the COR2 coronagraph FOV, this can be compared to Figure 5 which shows the eruption from the SolO/Metis perspective. The CME propagated to the south west, with a component travelling along the ecliptic plane. The COR2 image shown is actually indicative of a flux-rope structure inside the CME (see e.g., Cremades and Bothmer, 2004), in line with the sigmoid eruption observed by AIA.

The three dimensions (3D) geometric parameters of the CME can be constrained using the coronagraph data and applying a GCS model. The GCS model allows observations from different vantage points of the CME front to be fitted with a 3D shape resembling the outer envelope of a magnetic flux rope. For this process we used images from LASCO-C2, Metis, and COR2. The derived parameters are provided in Table 1. Figure 9 shows representative running difference images of the CME taken at three times (bottom), the top panels show the reconstructed 3D shape overlaid as a green mesh. This event is captured as a very faint partial halo CME by LASCO C2, with no clear signature in the C3 FOV. From the STEREO-A spacecraft perspective the event can clearly be seen above the west limb. Metis captured the initial phase of the eruption, but the CME exited the FOV after one frame. The results in Table 1 indicate that the CME propagated towards the Earth in the Heliocentric Earth Equatorial (HEEQ) longitude and 11° to the south of the solar equatorial plane.

Table 1. 3D CME geometrical parameters constrained by the GCS fitting (see Figure 9). The coordinate system used is HEEQ.

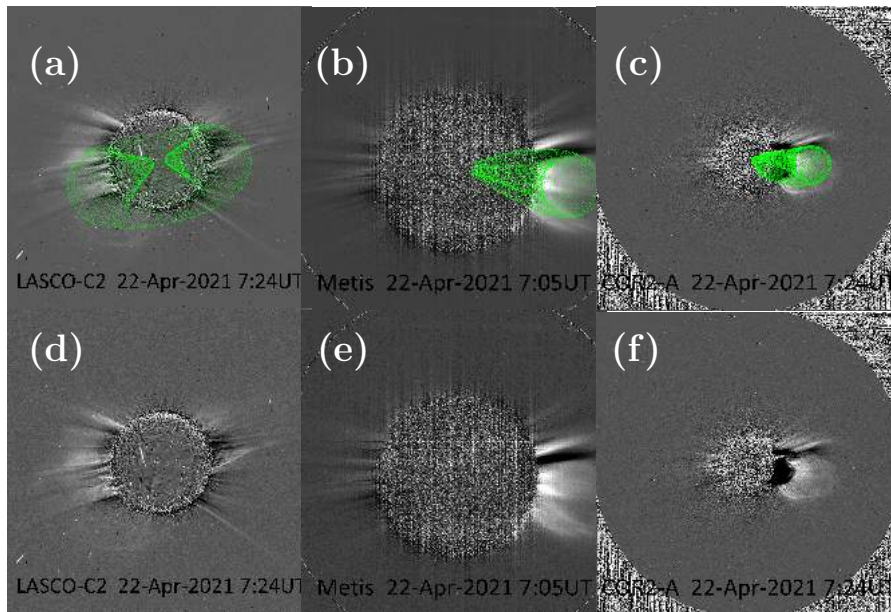| CME Parameter	Value
Latitude	$-11°$
Longitude	$0°$
Tilt angle	$12°$
Height	$[5.75,9.07]$ $R_\odot$
Aspect ratio	0.26
Half angle	$44°$
Speed	622 km s^{-1}

Figure 9. GCS fitting of the 22 April 2021 CME. Top panels show the fit (green mesh) overlaid on running difference images taken by SOHO/LASCO-C2 (a), SolO/Metis (b), and STEREO-A/COR2. The Bottom panels (d, e, and f) show the same running difference images used for the fitting without the mesh.

3. Flare observations

The Spectrometer/Telescope for Imaging X-rays (STIX) on SolO provides hard X-ray imaging spectroscopy measurements with a full-Sun field of view. STIX detects hard X-ray emission in the energy range of 4-150 keV, allowing diagnostics of both the hot thermal plasma in the solar corona as well as the accelerated non-thermal electrons accelerated during solar flares. Using Fourier-transform indirect imaging, STIX provides spatial information on angular scales of 7 to 180". With a spectral resolution of 1 keV (at 6 keV) and a temporal resolution
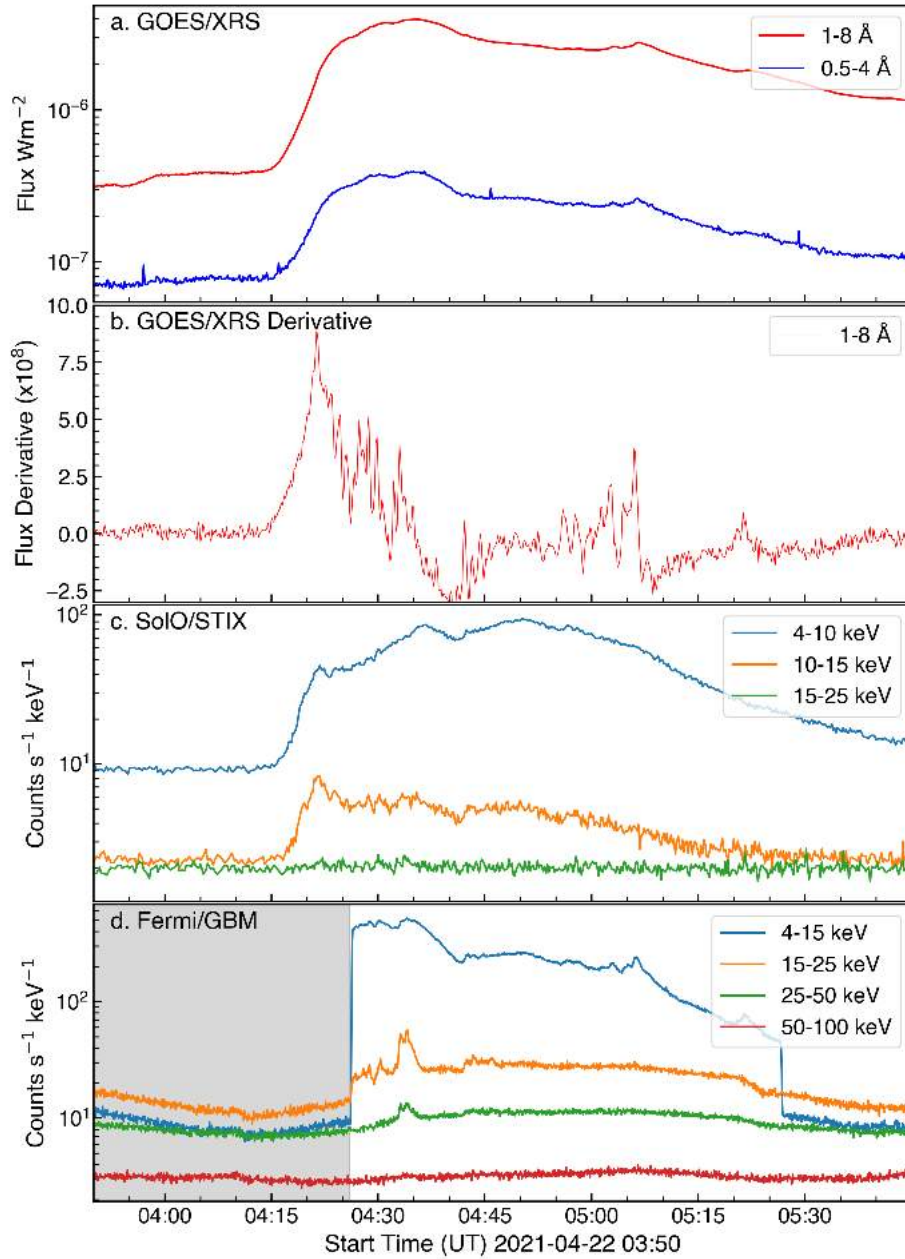
Figure 10. X-ray light curves of the solar flare associated with the eruption on 22 April 2021. The panels (from top to bottom) show: the GOES soft X-ray fluxes, the time derivative of the GOES 0.1-0.8 nm flux, the STIX X-ray count rates in three energy ranges, and the X-ray count rates as observed by Fermi-GBM in four channels (the shaded area shows the Fermi night). The STIX light curve is shifted by 68 s in time to account for the difference in light-travel time between SolO and Earth. Fermi only sees the Sun between 04:26 and 05:27 UT.

SDO/AIA 1600 22-Apr-2021 04:25:02.120 UT   SOLO/EUI/FSI 174 22-Apr-2021 04:24:00.303

Figure 11. Left: The flare as seen from near-Earth space with SDO/AIA in the 160 nm channel. The image uses an inverted color scale, where the flaring ribbons are clearly seen as dark structures. The overlaid green semicircle perpendicular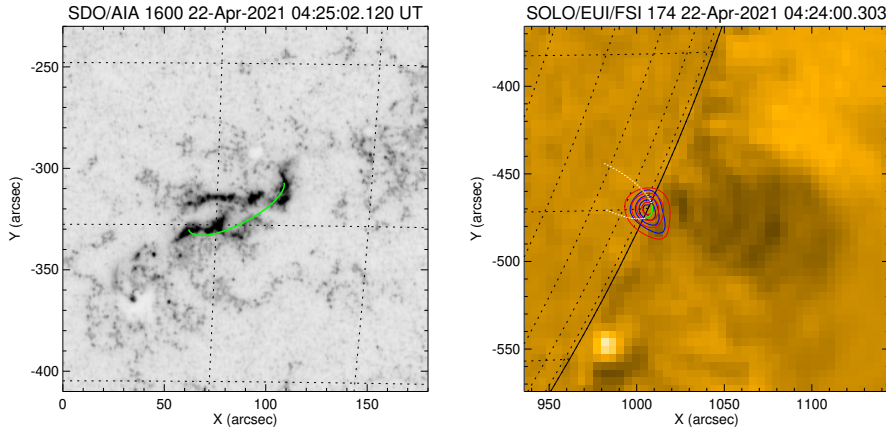 to the solar surface is shown as an indication of the 3D structure of the flare. Right: A SolO/EUI FSI 17.4 nm bandpass difference image (pre-image subtracted) of the flare. The semi-circle is the same as shown in the left panel, but seen from the SolO vantage point, where the visible portion of the semicircle is colored green, and the occulted portion white. The red and blue contours show the STIX X-ray sources at 6-10 keV and 10-15 keV, respectively.

as low as 0.5 s, STIX can quantify the location, intensity, spectrum, and timing of hot thermal plasma and accelerated electrons at the Sun.

STIX recorded an X-ray flare associated with the eruption. The STIX light curves are shown in the third panel of Figure 10. Corresponding context X-ray data obtained from near-Earth space can be seen in the top two panels, obtained from the GOES-16 satellite, as well as in the bottom panel, observed by the Fermi-GBM instrument Meegan *et al.* (2009). For better comparison between the near-Earth and STIX datasets, 68 seconds were added to STIX times in order to account for the difference in light travel time between SolO and Earth. In the following, all times indicated refer to UT at Earth.

The flare was classified as a GOES C3.8 flare, starting at 04:10 UT and peaking at 04:35 UT. Figure 10 shows that this was a long-duration event with multiple energy release episodes, as shown by the GOES derivative (second panel), which besides the main peak shows secondary peaks at 04:28 and 04:33 UT. The STIX light curves show corresponding peaks, especially in the 10-15 keV channel. The STIX light curves are quite unusual since they do not show significant emission above 15 keV. In contrast, the Fermi-GBM light curves clearly show multiple HXR bursts up to 50 keV. Since non-thermal emission is coming primarily from the flare loop footpoints, this suggests that the flare was partially occulted from the SolO perspective.

To investigate the viewing geometry in more detail, the left panel of Figure 11 shows the flare as seen from near-Earth space by AIA in the 160 nm channel. In green, we have overplotted a semi-circle perpendicular to the solar surface that connects the ribbons and gives some indication of the 3D extent of the flare.

The right panel of Figure 11 shows an EUI/FSI image at 17.4 nm from which a pre-event frame has been subtracted. The semi-circle is the same as shown on the left, but seen from the SolO vantage point (cf. Battaglia *et al.*, 2021). Note that only the top of the circle (green) is actually visible from SolO, while most of it is occulted (white points). The loop footpoints are located 12° behind the limb. Consequently, no bright flare signatures are seen in EUI. Instead, the corona above the semicircle shows an intensity depletion (coronal dimming), which is consistent with the expected mass loss due to the erupting CME. The red and blue contours show the STIX X-ray sources at 6-10 keV and 10-15 keV, respectively, integrated from 04:24 to 04:25 UT (at SolO), reconstructed with the MEM_GE imaging algorithm (Massa *et al.*, 2020).

At a heliocentric distance of 0.87 au, the STIX Aspect System (Warmuth *et al.*, 2020) is not functional, and therefore the exact position of the X-ray sources is not known precisely. However, we have applied an average image displacement obtained from other events observed from the cruise phase where aspect information was available. We estimate that this approach should result in a position uncertainty of about ±10". Indeed the location appears to be consistent with the 3D extent of the flare as approximated by the semicircle, as well as with the CME-related intensity depletion in EUI. We have thus established that STIX only sees the top part of the flaring loops, while most of the flare – in particular the non-thermal footpoints – remains occulted. We note that these flaring loops are initially not detected by EUI, presumably because they are too hot. However, after an EUI data gap between 04:55 UT and 06:01 UT, postflare loops are indeed seen at both 17.4 nm and 30.4 nm, when the flare plasma has cooled down sufficiently.

With this knowledge, we revisit the question of whether STIX has actually measured non-thermal emission, which for this flare must have originated from the corona. We therefore made a spectral analysis of the STIX data using the OSPEX SSWIDL package[3]. We forward-fitted the observed count spectra with the combination of an isothermal plasma component and a broken photon power-law with a fixed slope of -1.5 below the break that reproduces the non-thermal component (cf. Holman, 2003). Figure 12 shows time series of the fit parameters. The two topmost panels show emission measure (EM) and temperature of the thermal component. The error bars indicate the 1-sigma uncertainties. For comparison, the parameters from an isothermal fit of the GOES SXR fluxes are shown in orange. Note that STIX initially shows significantly higher temperatures and lower EM as compared to GOES. This behavior has been noted before and can be interpreted in terms of the different temperature responses of the SXR and HXR instruments (Battaglia *et al.*, 2021). STIX is more sensitive to hotter plasmas as compared to GOES, thus fitting the spectrum of a multithermal plasma with an isothermal component will give higher temperatures in STIX. This is most pronounced during the impulsive phase, while the parameters agree more closely in the decay phase of the flare, implying that the differential emission measure (DEM) of the flare plasma is equally well sampled by STIX and GOES. In this case, after 05:00 UT the parameters are basically equal within the uncertainties.
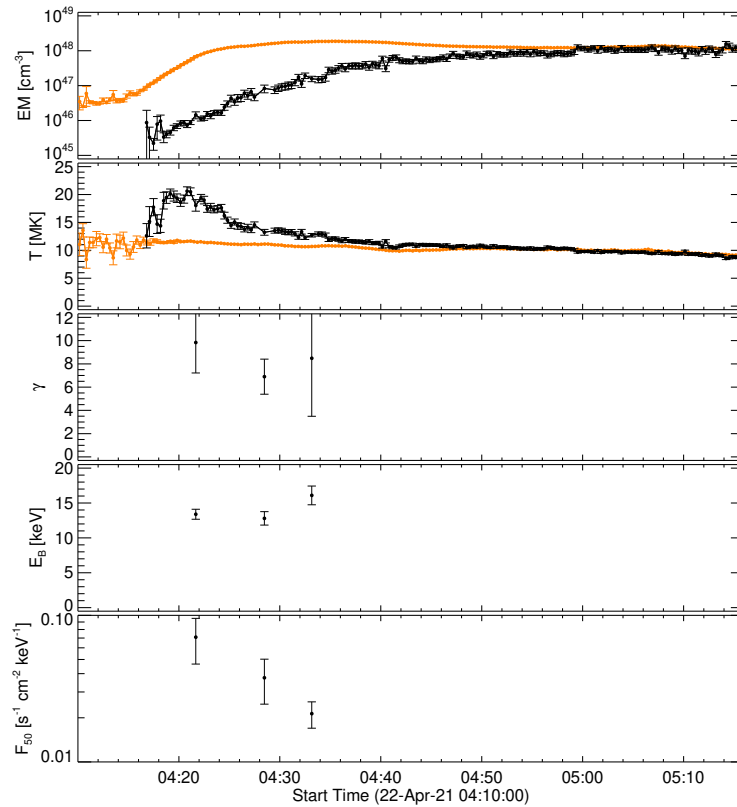
---

[3]http://hesperia.gsfc.nasa.gov/ssw/packages/spex/doc/

Figure 12. Time series of the parameters obtained from forward-fitting the STIX HXR spectra with the combination of an isothermal component and a photon power-law. Shown are emission measure and temperature of the thermal plasma, the spectral index γ, break energy E_{B}, and photon flux at 50 keV, F_{50}. For comparison, the EM and temperature obtained from the GOES data are shown in orange. The STIX times have been shifted to be consistent with the GOES observations from 1 au.

There are two other unusual thermal characteristics: The GOES temperature remains remarkably constant during the event, with no pronounced peak during the impulsive phase and a very gradual cooling phase (from 12 MK to 9 MK in one hour). This suggests that sustained heating must have been present even during the late phase of the flare. The other unusual behavior is that while the GOES EM peaks at 04:33 UT, the STIX EM continues to increase for another 30 min until it peaks. This can be explained by continuous magnetic reconnection which results in the formation of successively larger flaring loops that become filled with the plasma evaporated from the chromosphere. In effect, the fraction of the plasma that is seen by STIX is increasing, until from 05:00 UT onwards, STIX and GOES appear to be observing the same plasma.

With respect to non-thermal emission, there are only three brief episodes where a power-law component can be detected. They coincide with the first three peaks in the STIX light curves and the GOES derivative (cf. Figure 10).
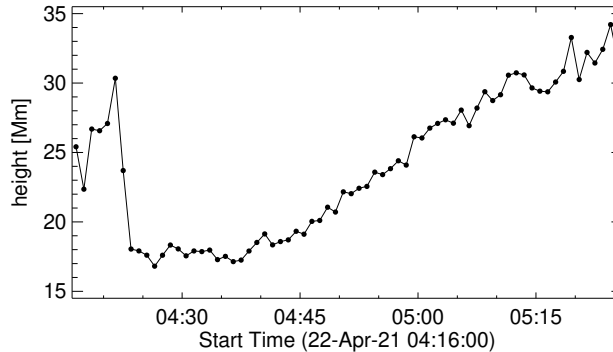
Figure 13. Deprojected height of the centroid of the STIX thermal source (6-10 keV) above the photosphere as a function of time. An occultation angle of 12° is assumed.

With slopes between 7 and 10, the spectra are very steep. While coronal non-thermal sources are well known to have softer spectra than the chromospheric footpoints, this event is in the softest range of the distribution (cf. Krucker and Lin, 2008; Effenberger *et al.*, 2017). Taking 20 Mm as the typical X-ray source size and assuming a filling factor of unity, the electron density of the thermal plasma at the non-thermal peaks can be estimated as 2×10^9, 6×10^9, and 1.1×10^{10} cm^{-3}, respectively. This corresponds to column densities N_c of 4×10^{18}, 1.2×10^{19}, and 2.2×10^{19} cm^{-2}. The thermal source is therefore able to stop electrons with energies of $E = (10^{-17} N_c)^{1/2}$ (Veronig and Brown, 2004; Krucker and Lin, 2008), in our case 6, 11 and 15 keV. This implies that at least the first non-thermal peak has to be dominated by thin-target bremsstrahlung, while there may have been a thick-target contribution in the two later peaks.

The notion of continuous reconnection that is suggested by the evolution of the EM and temperature is supported by the motion of the coronal X-ray source. Accounting for projection effects (the flare is occulted by 12°), we plot the height of the source centroid above the photosphere as a function of time in Figure 13. The derived heights are consistent with the typical height range of active region loops that have been determined from stereoscopy (cf. Rodriguez *et al.*, 2009). Initially, the source moves downward, which can be interpreted in terms of initially contracting loops (Veronig *et al.*, 2006; Warmuth and Mann, 2013) or an apparent motion due to increasing contribution of evaporated plasma (Warmuth and Mann, 2016). From 04:40 UT on, the source rises steadily at a speed of 6 km s^{-1}. This is consistent with the formation of large hot flare loops by continuous reconnection, while the plasma in the smaller loops cools out of the STIX passband.

4. In situ observations

Figure 14 is a screenshot from an animation (available in the online version) in which several CME fronts are modelled using the STEREO-A Heliospheric
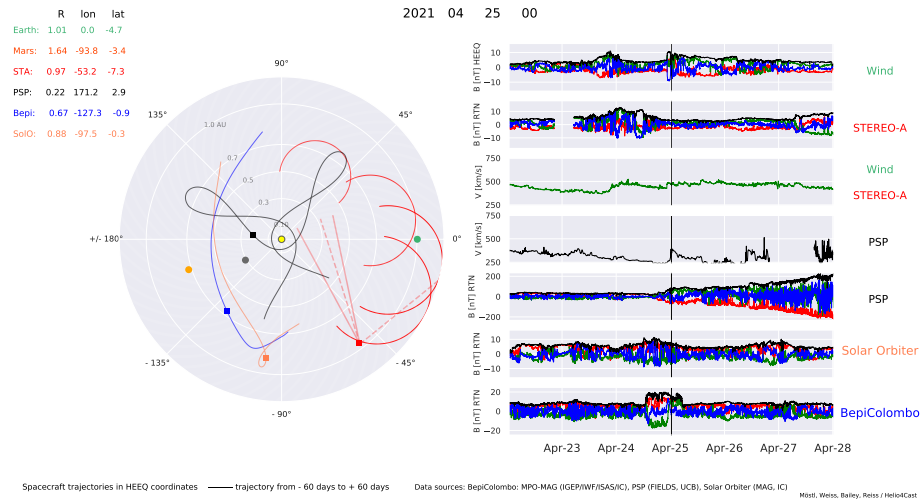
Figure 14. Frame from an animation (available in the online version) visualizing the 22 April 2021 eruption tracked with heliospheric imagers (on 25 April 2021, close to the arrival time to Earth). Left panel: A visualization of the inner heliosphere with the position and trajectory of several spacecraft (squares), celestial bodies (circles), and several CME fronts present at the time (red semi-circles, including the 22 April 2021 CME which is arriving to the Earth). The following spacecraft and celestial bodies are included: PSP (black), BepiColombo (blue), STEREO-A (red), the Sun (yellow), the Earth (green), and Mars (orange). The field of views of the STEREO-A/HI instruments are indicated by red solid (HI1) and dashed (HI2) lines. The red semi-circle indicates the position of the CME front on 25 April 2021, as recorded by the SSEF30 modeling. Right panel: from top to bottom show (with labels on the right side): the Wind magnetic-field measurements (in HEEQ coordinates; Bt black, Bx red, By green, Bz blue); the STEREO-A magnetic field in RTN (Radial Tangential Normal) coordinates (Bt black, Br red, Bt green, Bn blue); the STEREO-A and Wind bulk plasma speed; the PSP bulk plasma speed; and the bottom three panels how the PSP, SolO, and BepiColombo magnetic-field observations in RTN coordinates respectively. A full animation showing the changing parameters with time is available in the online version of the paper.

Imager (HI; Eyles *et al.*, 2009) observations and in situ data. The HI instruments have provided a new perspective on the inner heliosphere, helping to reveal the nature of solar-wind and CMEs (Harrison *et al.*, 2018; Rodriguez *et al.*, 2022, e.g.). On early 25 April the CME front (from the the 22 April eruption) impacted Earth, where elevated total magnetic field levels were recorded at Wind. The eruption was tracked with STEREO-A/HI and modelled using the self-similar expansion geometrical fitting model with 30° half width (SSEF30 model Davies *et al.*, 2012), as described in Möstl *et al.* (2022).

Measurements of the interplanetary plasma conditions at the Lagrangian point L1, from the Wind spacecraft, are shown in Figure 15, where weak ICME signatures (Kilpua, Koskinen, and Pulkkinen, 2017b) are detected. The vertical solid line on 24 April 2021 at 22:28:30 UT indicates the arrival of an interplanetary fast forward shock. This corresponds well with that predicted by the SSEF30 model (see Figure 14). At the shock the magnetic field magnitude, solar wind speed and other plasma parameters jump. A modest temperature increase is observed about 1.5 hours later, followed by a subsequent larger tempera-

ture jump. The shock was found to be quasi-perpendicular, relatively slow, and weak. Using the shock normal derived from the mixed mode method (Abraham-Shrauner, 1972; Abraham-Shrauner and Yun, 1976) gives a shock angle of 83.9°, the shock speed of 495 km s^{-1} and the Alfvén Mach number 1.9. The upstream and downstream intervals of 4 minutes were used in the analysis. Using these intervals the speed increase across the shock is found to be 50 km s^{-1}, the downstream to upstream magnetic field ratio is 1.76, and the density ratio is 2.04.

After the shock, the magnetic field direction fluctuates but there are no clear signatures of smooth rotations, which are typically observed in magnetic clouds with flux rope configurations. Nevertheless, the y component of the magnetic field, B_y, changes from positive to negative, and the B_x is clearly non-zero indicating a flank encounter. Starting from around 12:00 UT on 25 April, periods of decreased temperature (considered to be a key ICME signature) are observed. The structure preceding the shock observed on 23 April has signatures of a stream interaction region (SIR; e.g., Richardson, 2018), where the solar wind density and speed increase gradually. The stream interface between slow and faster wind shows a sharply decreasing density, and abruptly increasing temperature. The peak speed reached after the SIR is only ~ 500 km s^{-1}, i.e., it is not followed by fast stream.

Figure 16 shows magnetic field measurements from STEREO-A, that was located 53° away from the Sun-Earth line (see Figure 1). But, without plasma data (not available) it is difficult to make strong conclusions about the large-scale solar wind structures detected. However, on 24 April between 08:15 UT - 12:00 UT a period with smooth magnetic field and organized field rotation (indicated with an orange-shaded area in Figure 16) can be observed. In particular, the B_T component rotates smoothly from 5 nT to -10 nT. This structure lasts for less than four hours in duration, and indicates STEREO-A probably passed through the edge of an ICME. Nevertheless, we believe it is unlikely that this is the same ICME that was observed by Wind.

There are several pieces of evidence to indicate that the ICMEs observed at Wind and STEREO-A are different. Firstly, HI observes several CMEs propagating towards STEREO-A before the event on 22 April (see Figure 14 and the accompanying animation provided with the online version of this paper), each with slightly different kinematics. Furthermore, STEREO-A is quite far away from Earth (53° in longitude), and given that the CME source region is located near the disk center (from the Earth perspective), and the HI SSEF30 model estimates a propagation direction of W12S12, only a significant deflection near the Sun (of which there is no evidence), or an extremely wide CME could result in the eruption being detected at STEREO-A. Finally, there are no consistent in situ signatures observed between Wind and STEREO-A. For the aforementioned reasons, we can discard that STEREO-A and Wind saw the same CME, and this is a single-point in situ event, where the preceding interval of enhanced magnetic field, seen in STEREO-A, is likely a SIR, as the field is more variable.
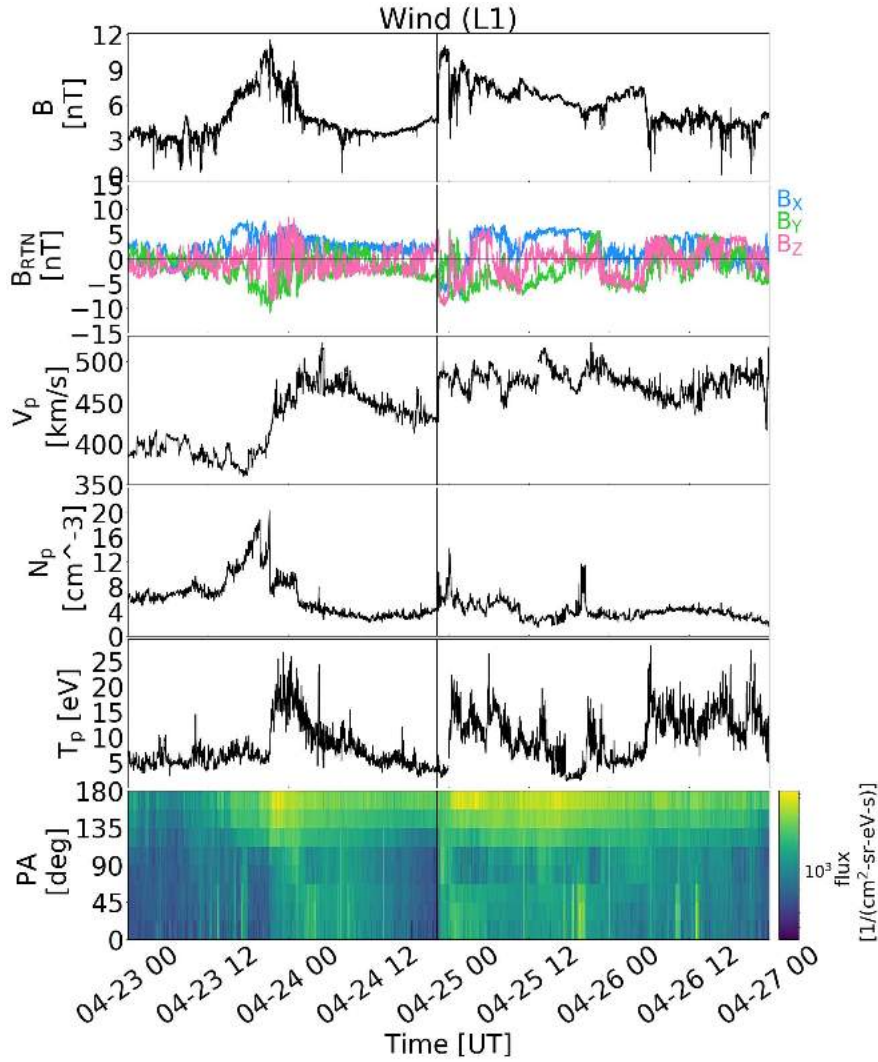
Figure 15. In-situ observations from the Wind spacecraft. The panels (from top to bottom) indicate: magnetic field magnitude; magnetic field magnitude in GSE coordinates; solar wind speed; solar wind density; solar wind temperature, and pitch angle of 427 eV electrons.

5. EUHFORIA simulations

The EUropean Heliospheric FORecasting Information Asset (EUHFORIA, Pomoell and Poedts, 2018) is a space weather forecasting-targeted inner heliosphere physics-based model. It consists of two coupled parts, a coronal model (which focuses on processes below 0.1 au) and a heliospheric model (which focuses on the heliosphere starting at 0.1 au). The first one uses synoptic magnetograms in order to compute the plasma parameters at 0.1 au using the Wang-Sheeley-Arge empirical model (WSA, Arge *et al.*, 2003). The second model takes as input the
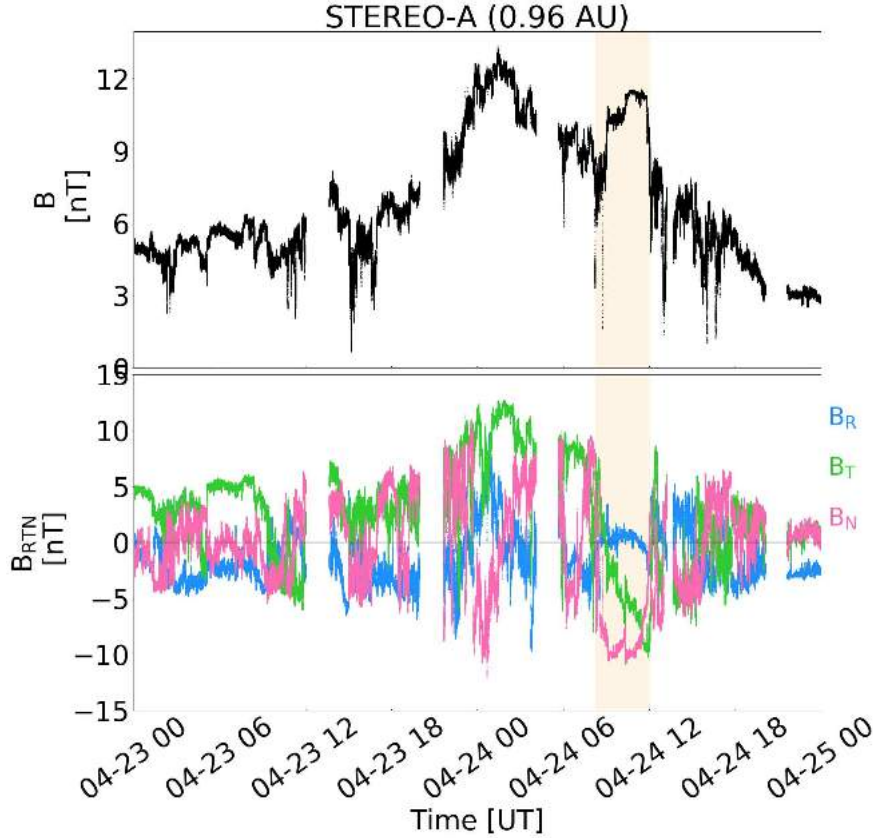
Figure 16. In-situ observations from STEREO-A. Top panel: magnetic field magnitude. Bottom panel: magnetic field measured in RTN components. The orange-shaded region indicates possible ICME material.

output at 0.1 au and it solves the 3D time-dependent ideal MHD equations in the HEEQ system for the whole domain, at a prescribed resolution. CMEs can be incorporated into the heliospheric simulation of EUHFORIA using different CME models, such as the simple cone model (Xie, Ofman, and Lawrence, 2004) which does not prescribe an internal magnetic field configuration for the CME and the more complex spheromak (Verbeke, Pomoell, and Poedts, 2019) and FRi3D models (Isavnin, 2016), which treat the CME as a flux rope. In this case, we used the cone and the spheromak models, they both produced similar results. This is because the Earth was intersected by the flank of the CME (see Section 4), there is no flux rope signature to be seen in the in situ data, making the use of a flux rope model not needed. Therefore, we show in this Section only the results of the cone model.

The EUHFORIA simulation of the 22 April 2021 event was made with a resolution of 512 grid cells in radial direction, and with 2° angular resolution. The cone model parameters are shown in Table 1 and the rest of the EUHFORIA paramenters in Table 2. We generated a relaxed background solar wind using

Table 2. CME input parameters used in EUH-FORIA simulations by modelling the CME with the cone model. The coordinate system used is HEEQ.

Input parameters	
CME model	Cone
Insertion time	2021-04-22T11:08
CME Speed	622 km s^{-1}
Latitude	$-11°$
Longitude	$0°$
Half Width	$44°$
Mass density	$1 \cdot 10^{-18}$ kg m^{-3}
Temperature	$0.8 \cdot 10^6$ K

magnetogram data provided by GONG, and optimized the output of the coronal model in order to reproduce the correct ambient solar wind, in which the CME was injected. For this purpose we explored different magnetograms within a 24-hour window from the time of the eruption, selecting the 21 April 2021, 21:00 UT observation as the best fit. The CME is then injected at 0.1 au onto this wind.

In Figure 17, the results of the simulation are shown and compared to the real data from OMNIWeb [4]. We use a network of virtual spacecraft located between $\pm5°$ and $\pm10°$ of latitude and longitude around Earth (shaded in blue in the figure). This is done in order to capture the variability of the simulation around the Earth. EUHFORIA simulates the arrival time of the ICME quite accurately (within 2 hours of the real arrival time). While the speed is slightly overestimated, the proton density and pressure are similar to the observed profiles. Since the CME is a flank encounter with the Earth, as described in Section 4, we do not observe a clear rotation of the magnetic field components, and consequently the magnetic field components are not modeled with EUHFORIA.

6. Summary and conclusions

In this paper, we presented a detailed analysis of the CME that erupted on 22 April 2021. This event was observed by the instruments onboard Solar Orbiter (at 0.87 au from the Sun), as well as by several other space-based assets. The eruption was seen at the southwest limb by SolO/EUI, with the source slightly backsided as seen from that perspective.

This event appears differently when compared to previous ones observed by Metis (Andretta *et al.*, 2021; Bemporad *et al.*, 2022). Here the UV image (Ly-α) seems less structured than the pB one. The events in the aforementioned studies

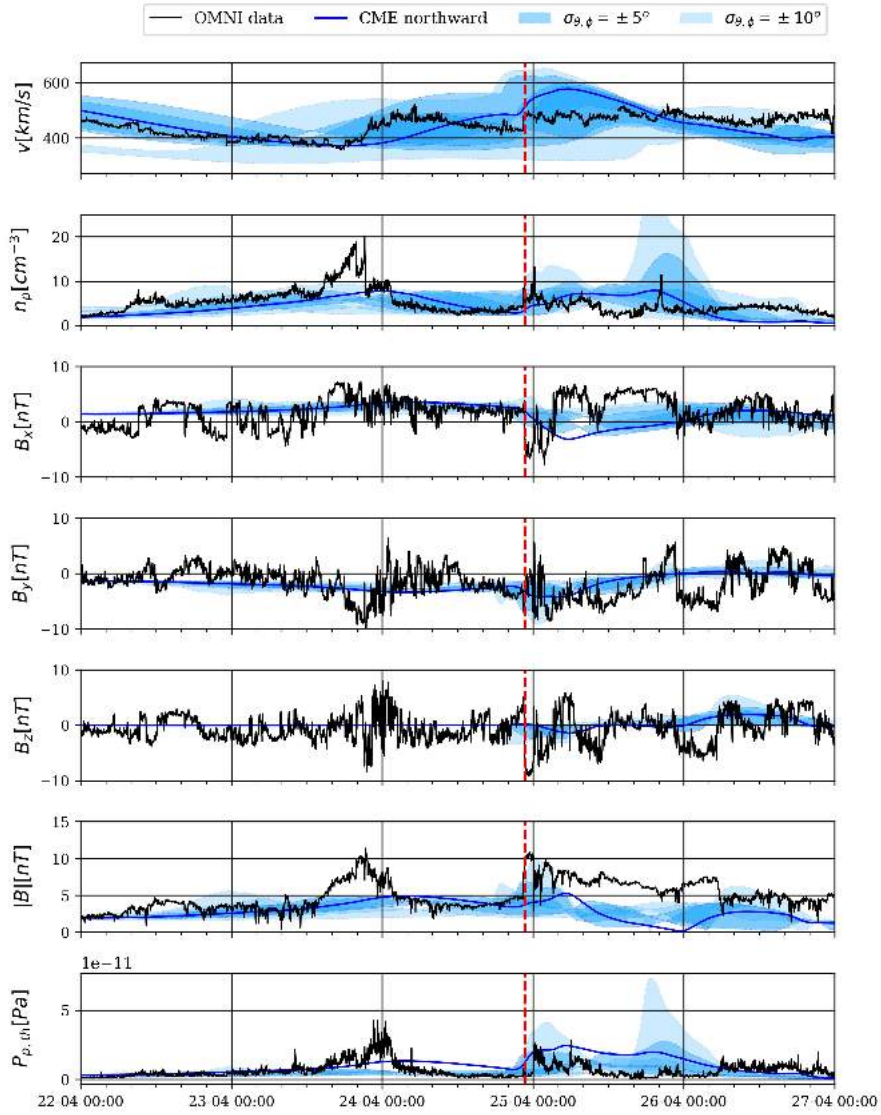---

[4]https://omniweb.gsfc.nasa.gov/

Figure 17. Measured and simulated solar wind properties at Earth between 22 April and 27 April 2021, capturing the arrival of the CME that emerged from the Sun on 22 April 2021. The panels (top to bottom) show: solar wind speed (v), proton density (n_p), magnetic field components B_x, B_y, B_z in GSE coordinates, magnetic field strength (B), and plasma beta (β). The blue solid line time series is obtained by injecting a cone CME. The dark and light shade of blue cover the variation of the time series recorded by the virtual satellites between ±5° and ±10° of latitude and longitude around Earth. Simulation results are compared to the 1-minute average in-situ solar wind measurements of the corresponding properties from OMNIWeb in black. The arrival time of the CME has been demarcated in red at 22:40 UT on 24 April 2021.

were detected at closer distances to the Sun (less than 0.6 au in both cases). This could be the result of a much reduced signal in the UV channel, possibly with some contribution of the interplanetary Ly-α, due to the different distances where the events are observed. It is also plausible that emission from the CME is significantly Doppler dimmed compared to the background corona.

The CME was associated with a solar flare that was observed in X-rays by STIX. The STIX X-ray lightcurves do not show significant emission above 15 keV. In contrast, Fermi-GBM clearly shows multiple HXR bursts up to 50 keV. Since non-thermal emission is coming primarily from the flare loop footpoints, this implies that the flare was partially occulted from the SolO perspective. Combining STIX and EUI observations, we established that STIX only sees the top part of the flaring loops, while most of the flare – in particular the non-thermal footpoints – remain occulted. We then determined, based on a comparison with GOES observations that sustained heating (ongoing energy release) must have been present even during the late phase of the flare. We also noticed that the STIX EM continues to increase after the GOES EM peaks, reaching a peak 30 minutes later. This can be explained by continuous magnetic reconnection, which results in the formation of successively larger flaring loops, that become filled by evaporated plasma. The growth of the loop system subsequently allows them to be observed above the solar limb by STIX. This is supported by the upward motion of the coronal X-ray source, which is consistent with the formation of successively larger postflare loops. With respect to non-thermal emission from the corona, there are only three brief episodes where a power-law component can be detected, with the first one dominated by thin target bremsstrahlung, while there may have been a thick-target contribution in the two later peaks.

The notion of continuous reconnection that is suggested by multiple lines of evidence from the STIX data is supported by the kinematics of the CME as measured by EUI (see Figure 4). The CME shows continuous acceleration, and indeed it is well known that CME acceleration tends to be correlated with the X-ray signatures of energy release (e.g. Zhang *et al.*, 2001). Accelerating a CME against gravity and aerodynamic drag requires energy input, and magnetic reconnection can provide this by reducing the downward-acting tension of the overlying field (Lin, 2004) and by adding poloidal magnetic flux to the erupting flux rope (Vršnak, 2008).

The eruption was observed close to disk center from the Earth perspective. PROBA2/SWAP and SDO/AIA observations revealed coronal dimmings and an EIT wave. SOHO/LASCO-C2 observed a partial halo CME starting around 06:00 UT. STEREO-A/COR2 recorded a clear structured CME seen from around 05:23 UT. The corresponding ICME arrived at the Earth late on 24 April 2021. It was driving a shock and created minor geomagnetic storm conditions. Most likely only a flank of the ICME hit the Earth, as the bulk of the CME was observed to be travelling southward. There was no clear flux-rope structure sampled in situ. The CME travel and consequent ICME arrival at Earth was modeled by EUHFORIA. In order to collect input parameters needed to run EUHFORIA, we combined data from SOHO/LASCO-C2, STEREO-A/COR2 and SolO/Metis. The model correctly predicts an arrival within 2 hours of the

observed one. The ICME is recognized in the simulated data by an increase in speed and density, and a slight increase in magnetic field.

This work highlights the importance of missions such as Solar Orbiter with a comprehensive suite of instruments that allow us to sample eruptions from a perspective other than that of the Earth. In particular, we have showcased the scientific potential that lies in combining data from Solar Orbiter and other space-based assets with state-of-the-art numerical modeling. We stress that the event discussed here was observed still during the cruise phase of Solar Orbiter, when many instruments were not operating at peak capacity yet. Significantly improved data quality is thus to be expected from the following science phase.

Appendix

References

Abraham-Shrauner, B.: 1972, Determination of magnetohydrodynamic shock normals. *J. Geophys. Res.* **77**(4), 736. DOI. ADS. [Abraham1972]

Abraham-Shrauner, B., Yun, S.H.: 1976, Interplanetary shocks seen by Ames Plasma Probe on Pioneer 6 and 7. *J. Geophys. Res.* **81**(13), 2097. DOI. ADS. [Abraham1976]

Andretta, V., Bemporad, A., De Leo, Y., Jerse, G., Landini, F., Mierla, M., Naletto, G., Romoli, M., Sasso, C., Slemer, A., Spadaro, D., Susino, R., Talpeanu, D.-C., Telloni, D., Teriaca, L., Uslenghi, M., Antonucci, E., Auchère, F., Berghmans, D., Berlicki, A., Capobianco, G., Capuano, G.E., Casini, C., Casti, M., Chioetto, P., Da Deppo, V., Fabi, M., Fineschi, S., Frassati, F., Frassetto, F., Giordano, S., Grimani, C., Heinzel, P., Liberatore, A., Magli, E., Massone, G., Messerotti, M., Moses, D., Nicolini, G., Pancrazzi, M., Pelizzo, M.-G., Romano, P., Schühle, U., Stangalini, M., Straus, T., Volpicelli, C.A., Zangrilli, L., Zuppella, P., Abbo, L., Aznar Cuadrado, R., Bruno, R., Ciaravella, A., D'Amicis, R., Lamy, P., Lanzafame, A., Malvezzi, A.M., Nicolosi, P., Nisticò, G., Peter, H., Plainaki, C., Poletto, L., Reale, F., Solanki, S.K., Strachan, L., Tondello, G., Tsinganos, K., Velli, M., Ventura, R., Vial, J.-C., Woch, J., Zimbardo, G.: 2021, The first coronal mass ejection observed in both visible-light and UV H I Ly-α channels of the Metis coronagraph on board Solar Orbiter. *Astron. Astrophys.* **656**, L14. DOI. ADS. [Andretta2021]

Antonucci, E., Romoli, M., Andretta, V., Fineschi, S., Heinzel, P., Moses, J.D., Naletto, G., Nicolini, G., Spadaro, D., Teriaca, L., Berlicki, A., Capobianco, G., Crescenzio, G., Da Deppo, V., Focardi, M., Frassetto, F., Heerlein, K., Landini, F., Magli, E., Marco Malvezzi, A., Massone, G., Melich, R., Nicolosi, P., Noci, G., Pancrazzi, M., Pelizzo, M.G., Poletto, L., Sasso, C., Schühle, U., Solanki, S.K., Strachan, L., Susino, R., Tondello, G., Uslenghi, M., Woch, J., Abbo, L., Bemporad, A., Casti, M., Dolei, S., Grimani, C., Messerotti, M., Ricci, M., Straus, T., Telloni, D., Zuppella, P., Auchère, F., Bruno, R., Ciaravella, A., Corso, A.J., Alvarez Copano, M., Aznar Cuadrado, R., D'Amicis, R., Enge, R., Gravina, A., Jejčič, S., Lamy, P., Lanzafame, A., Meierdierks, T., Papagiannaki, I., Peter, H., Fernandez Rico, G., Giday Sertsu, M., Staub, J., Tsinganos, K., Velli, M., Ventura, R., Verroi, E., Vial, J.-C., Vives, S., Volpicelli, A., Werner, S., Zerr, A., Negri, B., Castronuovo, M., Gabrielli, A., Bertacin, R., Carpentiero, R., Natalucci, S., Marliani, F., Cesa, M., Laget, P., Morea, D., Pieraccini, S., Radaelli, P., Sandri, P., Sarra, P., Cesare, S., Del Forno, F., Massa, E., Montabone, M., Mottini, S., Quattropani, D., Schillaci, T., Boccardo, R., Brando, R., Pandi, A., Baietto, C., Bertone, R., Alvarez-Herrero, A., García Parejo, P., Cebollero, M., Amoruso, M., Centonze, V.: 2020, Metis: the Solar Orbiter visible light and ultraviolet coronal imager. *Astron. Astrophys.* **642**, A10. DOI. ADS. [Antonucci2020]

Arge, C.N., Odstrcil, D., Pizzo, V.J., Mayer, L.R.: 2003, Improved Method for Specifying Solar Wind Speed Near the Sun. In: Velli, M., Bruno, R., Malara, F., Bucci, B. (eds.) *Solar Wind Ten*, *American Institute of Physics Conference Series* **679**, 190. DOI. ADS. [2003Arge]

Battaglia, A.F., Saqri, J., Massa, P., Perracchione, E., Dickson, E.C.M., Xiao, H., Veronig, A.M., Warmuth, A., Battaglia, M., Hurford, G.J., Meuris, A., Limousin, O., Etesi, L., Maloney, S.A., Schwartz, R.A., Kuhar, M., Schuller, F., Senthamizh Pavai, V., Musset, S., Ryan, D.F., Kleint, L., Piana, M., Massone, A.M., Benvenuto, F., Sylwester, J., Litwicka, M., Stęślicki, M., Mrozek, T., Vilmer, N., Fárník, F., Kašparová, J., Mann, G., Gallagher, P.T., Dennis, B.R., Csillaghy, A., Benz, A.O., Krucker, S.: 2021, STIX X-ray microflare observations during the Solar Orbiter commissioning phase. *Astron. Astrophys.* **656**, A4. DOI. ADS. [Battaglia2021]

Bemporad, A., Pagano, P., Giordano, S.: 2018, Measuring the electron temperatures of coronal mass ejections with future space-based multi-channel coronagraphs: a numerical test. *Astron. Astrophys.* **619**, A25. DOI. ADS. [Bemporad-etal:2018]

Bemporad, A., Andretta, V., Susino, R., Mancuso, S., Spadaro, D., Mierla, M., Berghmans, D., D'Huys, E., Zhukov, A.N., Talpeanu, D.-C., Colaninno, R., Hess, P., Koza, J., Jejcic, S., Heinzel, P., Antonucci, E., Da Deppo, V., Fineschi, S., Frassati, F., Jerse, G., Landini, F., Naletto, G., Nicolini, G., Pancrazzi, M., Romoli, M., Sasso, C., Slemer, A., Stangalini, M., Teriaca, L.: 2022, A Coronal Mass Ejection followed by a prominence eruption and a plasma blob as observed by Solar Orbiter. *arXiv e-prints*, arXiv:2202.10294. ADS. [Bemporad-etal:2022]

Benz, A.O.: 2017, Flare Observations. *Living Reviews in Solar Physics* **14**(1), 2. DOI. ADS. [Benz2017]

Brueckner, G.E., Howard, R.A., Koomen, M.J., Korendyke, C.M., Michels, D.J., Moses, J.D., Socker, D.G., Dere, K.P., Lamy, P.L., Llebaria, A., Bout, M.V., Schwenn, R., Simnett, G.M., Bedford, D.K., Eyles, C.J.: 1995, The Large Angle Spectroscopic Coronagraph (LASCO). *Solar Phys.* **162**(1-2), 357. DOI. ADS. [brueckner1995]

Cremades, H., Bothmer, V.: 2004, On the three-dimensional configuration of coronal mass ejections. *Astron. Astrophys.* **422**(1), 307. DOI. [2004Cremades]

Davies, E.E., Möstl, C., Owens, M.J., Weiss, A.J., Amerstorfer, T., Hinterreiter, J., Bauer, M., Bailey, R.L., Reiss, M.A., Forsyth, R.J., Horbury, T.S., O'Brien, H., Evans, V., Angelini, V., Heyner, D., Richter, I., Auster, H.-U., Magnes, W., Baumjohann, W., Fischer, D., Barnes, D., Davies, J.A., Harrison, R.A.: 2021, In situ multi-spacecraft and remote imaging observations of the first CME detected by Solar Orbiter and BepiColombo. *Astron. Astrophys.* **656**, A2. DOI. ADS. [Davies2021]

Davies, J.A., Harrison, R.A., Rouillard, A.P., Sheeley, N.R., Perry, C.H., Bewsher, D., Davis, C.J., Eyles, C.J., Crothers, S.R., Brown, D.S.: 2009, A synoptic view of solar transient evolution in the inner heliosphere using the Heliospheric Imagers on STEREO. *Geophys. Res. Lett.* **36**(2), L02102. DOI. ADS. [Davies2009]

Davies, J.A., Harrison, R.A., Perry, C.H., Möstl, C., Lugaz, N., Rollett, T., Davis, C.J., Crothers, S.R., Temmer, M., Eyles, C.J., Savani, N.P.: 2012, A Self-similar Expansion Model for Use in Solar Wind Transient Propagation Studies. *Astrophys. J.* **750**(1), 23. DOI. ADS. [Davies2012]

Delaboudinière, J.-P., Artzner, G.E., Brunaud, J., Gabriel, A.H., Hochedez, J.F., Millier, F., Song, X.Y., Au, B., Dere, K.P., Howard, R.A., Kreplin, R., Michels, D.J., Moses, J.D., Defise, J.M., Jamar, C., Rochus, P., Chauvineau, J.P., Marioge, J.P., Catura, R.C., Lemen, J.R., Shing, L., Stern, R.A., Gurman, J.B., Neupert, W.M., Maucherat, A., Clette, F., Cugnon, P., van Dessel, E.L.: 1995, EIT: Extreme-Ultraviolet Imaging Telescope for the SOHO Mission. *Solar Phys.* **162**, 291. DOI. ADS. [Delaboudiniere95]

Dissauer, K., Veronig, A.M., Temmer, M., Podladchikova, T., Vanninathan, K.: 2018, Statistics of Coronal Dimmings Associated with Coronal Mass Ejections. I. Characteristic Dimming Properties and Flare Association. *Astrophys. J.* **863**(2), 169. DOI. ADS. [Dissauer2018]

Dolei, S., Susino, R., Sasso, C., Bemporad, A., Andretta, V., Spadaro, D., Ventura, R., Antonucci, E., Abbo, L., Da Deppo, V., Fineschi, S., Focardi, M., Frassetto, F., Giordano, S., Landini, F., Naletto, G., Nicolini, G., Nicolosi, P., Pancrazzi, M., Romoli, M., Telloni, D.: 2018, Mapping the solar wind HI outflow velocity in the inner heliosphere by coronagraphic ultraviolet and visible-light observations. *Astron. Astrophys.* **612**, A84. DOI. ADS. [Dolei-etal:2018]

Domingo, V., Fleck, B., Poland, A.I.: 1995, The SOHO Mission: an Overview. *Solar Phys.* **162**(1-2), 1. DOI. ADS. [Domingo1995]

Dryer, M., Liou, K., Wu, C., Wu, S., Rich, N., Plunkett, S.P., Simpson, L., Fry, C.D., Schenk, K.: 2012, Extreme Fast Coronal Mass Ejection on 23 July 2012. In: *AGU Fall Meeting Abstracts* **2012**, SH44B. ADS. [Dryer2012]

Effenberger, F., Rubio da Costa, F., Oka, M., Saint-Hilaire, P., Liu, W., Petrosian, V., Glesener, L., Krucker, S.: 2017, Hard X-Ray Emission from Partially Occulted Solar Flares: RHESSI Observations in Two Solar Cycles. *Astrophys. J.* **835**(2), 124. DOI. ADS. [Effenberger2017]

Eyles, C.J., Harrison, R.A., Davis, C.J., Waltham, N.R., Shaughnessy, B.M., Mapson-Menard, H.C.A., Bewsher, D., Crothers, S.R., Davies, J.A., Simnett, G.M., Howard, R.A., Moses, J.D., Newmark, J.S., Socker, D.G., Halain, J.-P., Defise, J.-M., Mazy, E., Rochus, P.: 2009, The Heliospheric Imagers Onboard the STEREO Mission. *Solar Phys.* **254**(2), 387. DOI. ADS. [Eyles2009]

Fletcher, L., Dennis, B.R., Hudson, H.S., Krucker, S., Phillips, K., Veronig, A., Battaglia, M., Bone, L., Caspi, A., Chen, Q., Gallagher, P., Grigis, P.T., Ji, H., Liu, W., Milligan, R.O., Temmer, M.: 2011, An Observational Overview of Solar Flares. *Space Sci. Rev.* **159**(1-4), 19. DOI. ADS. [Fletcher2011]

Freiherr von Forstner, J.L., Dumbović, M., Möstl, C., Guo, J., Papaioannou, A., Elftmann, R., Xu, Z., Christoph Terasa, J., Kollhoff, A., Wimmer-Schweingruber, R.F., Rodríguez-Pacheco, J., Weiss, A.J., Hinterreiter, J., Amerstorfer, T., Bauer, M., Belov, A.V., Abunina, M.A., Horbury, T., Davies, E.E., O'Brien, H., Allen, R.C., Bruce Andrews, G., Berger, L., Boden, S., Cernuda Cangas, I., Eldrum, S., Espinosa Lara, F., Gómez Herrero, R., Hayes, J.R., Ho, G.C., Kulkarni, S.R., Jeffrey Lees, W., Martín, C., Mason, G.M., Pacheco, D.,

Prieto Mateo, M., Ravanbakhsh, A., Rodríguez Polo, O., Sánchez Prieto, S., Schlemm, C.E., Seifert, H., Tyagi, K., Yedla, M.: 2021, Radial evolution of the April 2020 stealth coronal mass ejection between 0.8 and 1 AU. Comparison of Forbush decreases at Solar Orbiter and near the Earth. *Astron. Astrophys.* **656**, A1. DOI. ADS. [Freiherr2021]

Giordano, S., Ciaravella, A., Raymond, J.C., Ko, Y.-K., Suleiman, R.: 2013, UVCS/SOHO catalog of coronal mass ejections from 1996 to 2005: Spectroscopic proprieties. *Journal of Geophysical Research (Space Physics)* **118**(3), 967. DOI. ADS. [Giordano-etal:2013]

Green, L.M., Török, T., Vršnak, B., Manchester, W., Veronig, A.: 2018, The Origin, Early Evolution and Predictability of Solar Eruptions. *Space Sci. Rev.* **214**(1), 46. DOI. ADS. [Green2018]

Halain, J.-P., Berghmans, D., Seaton, D.B., Nicula, B., De Groof, A., Mierla, M., Mazzoli, A., Defise, J.-M., Rochus, P.: 2013, The SWAP EUV Imaging Telescope. Part II: In-flight Performance and Calibration. *Solar Phys.* **286**(1), 67. DOI. ADS. [Halain2013]

Harrison, R.A., Davies, J.A., Barnes, D., Byrne, J.P., Perry, C.H., Bothmer, V., Eastwood, J.P., Gallagher, P.T., Kilpua, E.K.J., Möstl, C., Rodriguez, L., Rouillard, A.P., Odstrčil, D.: 2018, CMEs in the Heliosphere: I. A Statistical Analysis of the Observational Properties of CMEs Detected in the Heliosphere from 2007 to 2017 by STEREO/HI-1. *Solar Phys.* **293**, 77. DOI. ADS. [2018Harrison]

Holman, G.D.: 2003, The Effects of Low- and High-Energy Cutoffs on Solar Flare Microwave and Hard X-Ray Spectra. *Astrophys. J.* **586**(1), 606. DOI. ADS. [Holman2003]

Howard, R.A., Michels, D.J., Sheeley, J. N. R., Koomen, M.J.: 1982, The observation of a coronal transient directed at Earth. *Astrophys. J. Lett.* **263**, L101. DOI. ADS. [Howard1982]

Howard, R.A., Moses, J.D., Vourlidas, A., Newmark, J.S., Socker, D.G., Plunkett, S.P., Korendyke, C.M., Cook, J.W., Hurley, A., Davila, J.M., Thompson, W.T., St Cyr, O.C., Mentzell, E., Mehalick, K., Lemen, J.R., Wuelser, J.P., Duncan, D.W., Tarbell, T.D., Wolfson, C.J., Moore, A., Harrison, R.A., Waltham, N.R., Lang, J., Davis, C.J., Eyles, C.J., Mapson-Menard, H., Simnett, G.M., Halain, J.P., Defise, J.M., Mazy, E., Rochus, P., Mercier, R., Ravet, M.F., Delmotte, F., Auchere, F., Delaboudiniere, J.P., Bothmer, V., Deutsch, W., Wang, D., Rich, N., Cooper, S., Stephens, V., Maahs, G., Baugh, R., McMullin, D., Carter, T.: 2008, Sun Earth Connection Coronal and Heliospheric Investigation (SECCHI). *Space Sci. Rev.* **136**(1-4), 67. DOI. ADS. [Howard2008]

Hundhausen, A.J., Burkepile, J.T., St. Cyr, O.C.: 1994, Speeds of coronal mass ejections: SMM observations from 1980 and 1984-1989. *J. Geophys. Res.* **99**, 6543. DOI. ADS. [Hundhausen1994]

Isavnin, A.: 2016, FRiED: A Novel Three-dimensional Model of Coronal Mass Ejections. *Astrophys. J.* **833**(2), 267. DOI. ADS. [Isavnin2016]

Kaiser, M.L., Kucera, T.A., Davila, J.M., St. Cyr, O.C., Guhathakurta, M., Christian, E.: 2008, The STEREO Mission: An Introduction. *Space Sci. Rev.* **136**(1-4), 5. DOI. ADS. [Kaiser2008]

Kilpua, E., Koskinen, H.E.J., Pulkkinen, T.I.: 2017a, Coronal mass ejections and their sheath regions in interplanetary space. *Living Reviews in Solar Physics* **14**(1), 5. DOI. ADS. [Kilpua2017LRSP]

Kilpua, E., Koskinen, H.E.J., Pulkkinen, T.I.: 2017b, Coronal mass ejections and their sheath regions in interplanetary space. *Living Reviews in Solar Physics* **14**(1), 5. DOI. ADS. [Kilpua2019]

Kilpua, E.K.J., Balogh, A., von Steiger, R., Liu, Y.D.: 2017, Geoeffective Properties of Solar Transients and Stream Interaction Regions. *Space Sci. Rev.* **212**(3-4), 1271. DOI. ADS. [Kilpua2017SSR]

Kilpua, E.K.J., Good, S.W., Dresing, N., Vainio, R., Davies, E.E., Forsyth, R.J., Gieseler, J., Lavraud, B., Asvestari, E., Morosan, D.E., Pomoell, J., Price, D.J., Heyner, D., Horbury, T.S., Angelini, V., O'Brien, H., Evans, V., Rodriguez-Pacheco, J., Gómez Herrero, R., Ho, G.C., Wimmer-Schweingruber, R.: 2021, Multi-spacecraft observations of the structure of the sheath of an interplanetary coronal mass ejection and related energetic ion enhancement. *Astron. Astrophys.* **656**, A8. DOI. ADS. [Kilpua2021]

Kohl, J.L., Noci, G., Antonucci, E., Tondello, G., Huber, M.C.E., Gardner, L.D., Nicolosi, P., Strachan, L., Fineschi, S., Raymond, J.C., Romoli, M., Spadaro, D., Panasyuk, A., Siegmund, O.H.W., Benna, C., Ciaravella, A., Cranmer, S.R., Giordano, S., Karovska, M., Martin, R., Michels, J., Modigliani, A., Naletto, G., Pernechele, C., Poletto, G., Smith, P.L.: 1997, First Results from the SOHO Ultraviolet Coronagraph Spectrometer. *Solar Phys.* **175**(2), 613. DOI. ADS. [Kohl-etal:1997]

Koskinen, H.E.J., Baker, D.N., Balogh, A., Gombosi, T., Veronig, A., von Steiger, R.: 2017, Achievements and Challenges in the Science of Space Weather. *Space Sci. Rev.* **212**(3-4), 1137. DOI. ADS. [Koskinen2017]

Kraaikamp, E., Verbeeck, C.: 2015, Solar Demon - an approach to detecting flares, dimmings, and EUV waves on SDO/AIA images. *Journal of Space Weather and Space Climate* **5**, A18. DOI. ADS. [Kraaikamp2015]

Krucker, S., Lin, R.P.: 2008, Hard X-Ray Emissions from Partially Occulted Solar Flares. *Astrophys. J.* **673**(2), 1181. DOI. ADS. [Krucker2008]

Krucker, S., Hurford, G.J., Grimm, O., Kögl, S., Gröbelbauer, H.-P., Etesi, L., Casadei, D., Csillaghy, A., Benz, A.O., Arnold, N.G., Molendini, F., Orleanski, P., Schori, D., Xiao, H., Kuhar, M., Hochmuth, N., Felix, S., Schramka, F., Marcin, S., Kobler, S., Iseli, L., Dreier, M., Wiehl, H.J., Kleint, L., Battaglia, M., Lastufka, E., Sathiapal, H., Lapadula, K., Bednarzik, M., Birrer, G., Stutz, S., Wild, C., Marone, F., Skup, K.R., Cichocki, A., Ber, K., Rutkowski, K., Bujwan, W., Juchnikowski, G., Winkler, M., Darmetko, M., Michalska, M., Seweryn, K., Białek, A., Osica, P., Sylwester, J., Kowalinski, M., Ścisłowski, D., Siarkowski, M., Steślicki, M., Mrozek, T., Podgórski, P., Meuris, A., Limousin, O., Gevin, O., Le Mer, I., Brun, S., Strugarek, A., Vilmer, N., Musset, S., Maksimović, M., Fárník, F., Kozáček, Z., Kašparová, J., Mann, G., Önel, H., Warmuth, A., Rendtel, J., Anderson, J., Bauer, S., Dionies, F., Paschke, J., Plüschke, D., Woche, M., Schuller, F., Veronig, A.M., Dickson, E.C.M., Gallagher, P.T., Maloney, S.A., Bloomfield, D.S., Piana, M., Massone, A.M., Benvenuto, F., Massa, P., Schwartz, R.A., Dennis, B.R., van Beek, H.F., Rodríguez-Pacheco, J., Lin, R.P.: 2020, The Spectrometer/Telescope for Imaging X-rays (STIX). *Astron. Astrophys.* **642**, A15. DOI. ADS. [Krucker20]

Lemen, J.R., Title, A.M., Akin, D.J., Boerner, P.F., Chou, C., Drake, J.F., Duncan, D.W., Edwards, C.G., Friedlaender, F.M., Heyman, G.F., Hurlburt, N.E., Katz, N.L., Kushner, G.D., Levay, M., Lindgren, R.W., Mathur, D.P., McFeaters, E.L., Mitchell, S., Rehse, R.A., Schrijver, C.J., Springer, L.A., Stern, R.A., Tarbell, T.D., Wuelser, J.-P., Wolfson, C.J., Yanari, C., Bookbinder, J.A., Cheimets, P.N., Caldwell, D., Deluca, E.E., Gates, R., Golub, L., Park, S., Podgorski, W.A., Bush, R.I., Scherrer, P.H., Gummin, M.A., Smith, P., Auker, G., Jerram, P., Pool, P., Soufli, R., Windt, D.L., Beardsley, S., Clapp, M., Lang, J., Waltham, N.: 2012, The Atmospheric Imaging Assembly (AIA) on the Solar Dynamics Observatory (SDO). *Solar Phys.* **275**(1-2), 17. DOI. ADS. [Lemen2012]

Lin, J.: 2004, CME-Flare Association Deduced from Catastrophic Model of CMEs. *Solar Phys.* **219**(1), 169. DOI. ADS. [Lin2004]

Liou, K., Wu, C.-C., Dryer, M., Wu, S.-T., Rich, N., Plunkett, S., Simpson, L., Fry, C.D., Schenk, K.: 2014, Global simulation of extremely fast coronal mass ejection on 23 july 2012. *Journal of Atmospheric and Solar-Terrestrial Physics* **121**, 32. DOI. https://www.sciencedirect.com/science/article/pii/S1364682614002247. [Liou2014]

Liu, W., Ofman, L.: 2014, Advances in Observing Various Coronal EUV Waves in the SDO Era and Their Seismological Applications (Invited Review). *Solar Phys.* **289**(9), 3233. DOI. ADS. [Liu2014]

Long, D.M., Bloomfield, D.S., Chen, P.F., Downs, C., Gallagher, P.T., Kwon, R.-Y., Vanninathan, K., Veronig, A.M., Vourlidas, A., Vršnak, B., Warmuth, A., Žic, T.: 2017, Understanding the Physical Nature of Coronal "EIT Waves". *Solar Phys.* **292**(1), 7. DOI. ADS. [Long2017]

Massa, P., Schwartz, R., Tolbert, A.K., Massone, A.M., Dennis, B.R., Piana, M., Benvenuto, F.: 2020, MEM_GE: A New Maximum Entropy Method for Image Reconstruction from Solar X-Ray Visibilities. *Astrophys. J.* **894**(1), 46. DOI. ADS. [Massa2020]

Meegan, C., Lichti, G., Bhat, P.N., Bissaldi, E., Briggs, M.S., Connaughton, V., Diehl, R., Fishman, G., Greiner, J., Hoover, A.S., van der Horst, A.J., von Kienlin, A., Kippen, R.M., Kouveliotou, C., McBreen, S., Paciesas, W.S., Preece, R., Steinle, H., Wallace, M.S., Wilson, R.B., Wilson-Hodge, C.: 2009, THEFERMIGAMMA-RAY BURST MONITOR. *The Astrophysical Journal* **702**(1), 791. DOI. https://doi.org/10.1088/0004-637x/702/1/791. [Meegan2009]

Morgan, H., Habbal, S.R., Woo, R.: 2006, The Depiction of Coronal Structure in White-Light Images. *Solar Phys.* **236**(2), 263. DOI. ADS. [Morgan-etal:2006]

Möstl, C., Weiss, A.J., Reiss, M.A., Amerstorfer, T., Bailey, R.L., Hinterreiter, J., Bauer, M., Barnes, D., Davies, J.A., Harrison, R.A., Freiherr von Forstner, J.L., Davies, E.E., Heyner, D., Horbury, T., Bale, S.D.: 2022, Multipoint Interplanetary Coronal Mass Ejections Observed with Solar Orbiter, BepiColombo, Parker Solar Probe, Wind, and STEREO-A. *Astrophys. J. Lett.* **924**(1), L6. DOI. ADS. [Moestl2022]

Müller, D., Nicula, B., Felix, S., Verstringe, F., Bourgoignie, B., Csillaghy, A., Berghmans, D., Jiggens, P., García-Ortiz, J.P., Ireland, J., Zahniy, S., Fleck, B.: 2017, JHelioviewer. Time-dependent 3D visualisation of solar and heliospheric data. *Astron. Astrophys.* **606**, A10. DOI. ADS. `[Mueller2017]`

Müller, D., St. Cyr, O.C., Zouganelis, I., Gilbert, H.R., Marsden, R., Nieves-Chinchilla, T., Antonucci, E., Auchère, F., Berghmans, D., Horbury, T.S., Howard, R.A., Krucker, S., Maksimovic, M., Owen, C.J., Rochus, P., Rodriguez-Pacheco, J., Romoli, M., Solanki, S.K., Bruno, R., Carlsson, M., Fludra, A., Harra, L., Hassler, D.M., Livi, S., Louarn, P., Peter, H., Schühle, U., Teriaca, L., del Toro Iniesta, J.C., Wimmer-Schweingruber, R.F., Marsch, E., Velli, M., De Groof, A., Walsh, A., Williams, D.: 2020, The Solar Orbiter mission. Science overview. *Astron. Astrophys.* **642**, A1. DOI. ADS. `[Mueller20]`

Möstl, C., Rollett, T., Lugaz, N., Farrugia, C.J., Davies, J.A., Temmer, M., Veronig, A.M., Harrison, R.A., Crothers, S., Luhmann, J.G., Galvin, A.B., Zhang, T.L., Baumjohann, W., Biernat, H.K.: 2011, ARRIVAL TIME CALCULATION FOR INTERPLANETARY CORONAL MASS EJECTIONS WITH CIRCULAR FRONTS AND APPLICATION TOSTEREOOBSERVATIONS OF THE 2009 FEBRUARY 13 ERUPTION. *The Astrophysical Journal* **741**(1), 34. DOI. https://doi.org/10.1088/0004-637x/741/1/34. `[Moestl_2011]`

O'Kane, J., Green, L.M., Davies, E.E., Möstl, C., Hinterreiter, J., Freiherr von Forstner, J.L., Weiss, A.J., Long, D.M., Amerstorfer, T.: 2021, Solar origins of a strong stealth CME detected by Solar Orbiter. *Astron. Astrophys.* **656**, L6. DOI. ADS. `[Okane2021]`

Pesnell, W.D., Thompson, B.J., Chamberlin, P.C.: 2012, The Solar Dynamics Observatory (SDO). *Solar Phys.* **275**(1-2), 3. DOI. ADS. `[Pesnell2012]`

Pomoell, J., Poedts, S.: 2018, EUHFORIA: European heliospheric forecasting information asset. *Journal of Space Weather and Space Climate* **8**, A35. DOI. ADS. `[Pomoell2018]`

Richardson, I.G.: 2018, Solar wind stream interaction regions throughout the heliosphere. *Living Reviews in Solar Physics* **15**(1), 1. DOI. ADS. `[Richardson2018]`

Robbrecht, E., Berghmans, D.: 2004, Automated recognition of coronal mass ejections (cmes) in near-real-time data. *A&A* **425**(3), 1097. DOI. https://doi.org/10.1051/0004-6361:20041302. `[2004Robbrecht]`

Rochus, P., Auchère, F., Berghmans, D., Harra, L., Schmutz, W., Schühle, U., Addison, P., Appourchaux, T., Aznar Cuadrado, R., Baker, D., Barbay, J., Bates, D., BenMoussa, A., Bergmann, M., Beurthe, C., Borgo, B., Bonte, K., Bouzit, M., Bradley, L., Büchel, V., Buchlin, E., Büchner, J., Cabé, F., Cadiergues, L., Chaigneau, M., Chares, B., Choque Cortez, C., Coker, P., Condamin, M., Coumar, S., Curdt, W., Cutler, J., Davies, D., Davison, G., Defise, J.-M., Del Zanna, G., Delmotte, F., Delouille, V., Dolla, L., Dumesnil, C., Dürig, F., Enge, R., François, S., Fourmond, J.-J., Gillis, J.-M., Giordanengo, B., Gissot, S., Green, L.M., Guerreiro, N., Guilbaud, A., Gyo, M., Haberreiter, M., Hafiz, A., Hailey, M., Halain, J.-P., Hansotte, J., Hecquet, C., Heerlein, K., Hellin, M.-L., Hemsley, S., Hermans, A., Hervier, V., Hochedez, J.-F., Houbrechts, Y., Ihsan, K., Jacques, L., Jérôme, A., Jones, J., Kahle, M., Kennedy, T., Klaproth, M., Kolleck, M., Koller, S., Kotsialos, E., Kraaikamp, E., Langer, P., Lawrenson, A., Le Clech', J.-C., Lenaerts, C., Liebecq, S., Linder, D., Long, D.M., Mampaey, B., Markiewicz-Innes, D., Marquet, B., Marsch, E., Matthews, S., Mazy, E., Mazzoli, A., Meining, S., Meltchakov, E., Mercier, R., Meyer, S., Monecke, M., Monfort, F., Morinaud, G., Moron, F., Mountney, L., Müller, R., Nicula, B., Parenti, S., Peter, H., Pfiffner, D., Philippon, A., Phillips, I., Plesseria, J.-Y., Pylyser, E., Rabecki, F., Ravet-Krill, M.-F., Rebellato, J., Renotte, E., Rodriguez, L., Roose, S., Rosin, J., Rossi, L., Roth, P., Rouesnel, F., Roulliay, M., Rousseau, A., Ruane, K., Scanlan, J., Schlatter, P., Seaton, D.B., Silliman, K., Smit, S., Smith, P.J., Solanki, S.K., Spescha, M., Spencer, A., Stegen, K., Stockman, Y., Szwec, N., Tamiatto, C., Tandy, J., Teriaca, L., Theobald, C., Tychon, I., van Driel-Gesztelyi, L., Verbeeck, C., Vial, J.-C., Werner, S., West, M.J., Westwood, D., Wiegelmann, T., Willis, G., Winter, B., Zerr, A., Zhang, X., Zhukov, A.N.: 2020, The Solar Orbiter EUI instrument: The Extreme Ultraviolet Imager. *Astron. Astrophys.* **642**, A8. DOI. ADS. `[Rochus2020...8R]`

Rodriguez, L., Zhukov, A.N., Gissot, S., Mierla, M.: 2009, Three-Dimensional Reconstruction of Active Regions. *Solar Phys.* **256**(1-2), 41. DOI. ADS. `[Rodriguez2009]`

Rodriguez, L., Zhukov, A.N., Cid, C., Cerrato, Y., Saiz, E., Cremades, H., Dasso, S., Menvielle, M., Aran, A., Mandrini, C., Poedts, S., Schmieder, B.: 2009, Three frontside full halo coronal mass ejections with a nontypical geomagnetic response. *Space Weather* **7**(6). DOI. https://agupubs.onlinelibrary.wiley.com/doi/abs/10.1029/2008SW000453. `[Rodriguez2009halos]`

Rodriguez, L., Mierla, M., Zhukov, A.N., West, M., Kilpua, E.: 2011, Linking Remote-Sensing and In Situ Observations of Coronal Mass Ejections Using STEREO. *Solar Phys.* **270**(2), 561. DOI. ADS. [Rodriguez2011]

Rodriguez, L., Scolini, C., Mierla, M., Zhukov, A.N., West, M.J.: 2020, Space Weather Monitor at the L5 Point: A Case Study of a CME Observed with STEREO B. *Space Weather* **18**(10), e02533. DOI. ADS. [Rodriguez2020]

Rodriguez, L., Barnes, D., Hosteaux, S., Davies, J.A., Willems, S., Pant, V., Harrison, R.A., Berghmans, D., Bothmer, V., Eastwood, J.P., Gallagher, P.T., Kilpua, E.K.J., Magdalenic, J., Mierla, M., Möstl, C., Rouillard, A.P., Odstrčil, D., Poedts, S.: 2022, Comparing the Heliospheric Cataloging, Analysis, and Techniques Service (HELCATS) Manual and Automatic Catalogues of Coronal Mass Ejections Using Solar Terrestrial Relations Observatory/Heliospheric Imager (STEREO/HI) Data. *Solar Phys.* **297**(2), 23. DOI. ADS. [Rodriguez2022]

Romoli, M., Antonucci, E., Andretta, V., Capuano, G.E., Da Deppo, V., De Leo, Y., Downs, C., Fineschi, S., Heinzel, P., Landini, F., Liberatore, A., Naletto, G., Nicolini, G., Pancrazzi, M., Sasso, C., Spadaro, D., Susino, R., Telloni, D., Teriaca, L., Uslenghi, M., Wang, Y.-M., Bemporad, A., Capobianco, G., Casti, M., Fabi, M., Frassati, F., Frassetto, F., Giordano, S., Grimani, C., Jerse, G., Magli, E., Massone, G., Messerotti, M., Moses, D., Pelizzo, M.-G., Romano, P., Schühle, U., Slemer, A., Stangalini, M., Straus, T., Volpicelli, C.A., Zangrilli, L., Zuppella, P., Abbo, L., Auchère, F., Aznar Cuadrado, R., Berlicki, A., Bruno, R., Ciaravella, A., D'Amicis, R., Lamy, P., Lanzafame, A., Malvezzi, A.M., Nicolosi, P., Nisticò, G., Peter, H., Plainaki, C., Poletto, L., Reale, F., Solanki, S.K., Strachan, L., Tondello, G., Tsinganos, K., Velli, M., Ventura, R., Vial, J.-C., Woch, J., Zimbardo, G.: 2021, First light observations of the solar wind in the outer corona with the Metis coronagraph. *Astron. Astrophys.* **656**, A32. DOI. ADS. [Romoli2021]

Santandrea, S., Gantois, K., Strauch, K., Teston, F., Tilmans, E., Baijot, C., Gerrits, D., De Groof, A., Schwehm, G., Zender, J.: 2013, PROBA2: Mission and Spacecraft Overview. *Solar Phys.* **286**(1), 5. DOI. ADS. [Santandrea2013]

Schwenn, R.: 2006, Space Weather: The Solar Perspective. *Living Reviews in Solar Physics* **3**(1), 2. DOI. ADS. [Schwenn2006]

Seaton, D.B., Berghmans, D., Nicula, B., Halain, J.-P., De Groof, A., Thibert, T., Bloomfield, D.S., Raftery, C.L., Gallagher, P.T., Auchère, F., Defise, J.-M., D'Huys, E., Lecat, J.-H., Mazy, E., Rochus, P., Rossi, L., Schühle, U., Slemzin, V., Yalim, M.S., Zender, J.: 2013, The SWAP EUV Imaging Telescope Part I: Instrument Overview and Pre-Flight Testing. *Solar Phys.* **286**(1), 43. DOI. ADS. [Seaton2013]

Telloni, D., Scolini, C., Möstl, C., Zank, G.P., Zhao, L.-L., Weiss, A.J., Reiss, M.A., Laker, R., Perrone, D., Khotyaintsev, Y., Steinvall, K., Sorriso-Valvo, L., Horbury, T.S., Wimmer-Schweingruber, R.F., Bruno, R., D'Amicis, R., De Marco, R., Jagarlamudi, V.K., Carbone, F., Marino, R., Stangalini, M., Nakanotani, M., Adhikari, L., Liang, H., Woodham, L.D., Davies, E.E., Hietala, H., Perri, S., Gómez-Herrero, R., Rodríguez-Pacheco, J., Antonucci, E., Romoli, M., Fineschi, S., Maksimovic, M., Souček, J., Chust, T., Kretzschmar, M., Vecchio, A., Müller, D., Zouganelis, I., Winslow, R.M., Giordano, S., Mancuso, S., Susino, R., Ivanovski, S.L., Messerotti, M., O'Brien, H., Evans, V., Angelini, V.: 2021, Study of two interacting interplanetary coronal mass ejections encountered by Solar Orbiter during its first perihelion passage. Observations and modeling. *Astron. Astrophys.* **656**, A5. DOI. ADS. [Telloni2021]

Temmer, M.: 2021, Space weather: the solar perspective. *Living Reviews in Solar Physics* **18**(1), 4. DOI. ADS. [Temmer2021]

Thernisien, A.: 2011, Implementation of the Graduated Cylindrical Shell Model for the Three-dimensional Reconstruction of Coronal Mass Ejections. *Astrophysical Journal Supplement* **194**(2), 33. DOI. ADS. [Thernisien2011]

Thompson, B.J., Plunkett, S.P., Gurman, J.B., Newmark, J.S., St. Cyr, O.C., Michels, D.J.: 1998, SOHO/EIT observations of an Earth-directed coronal mass ejection on May 12, 1997. *Geophys. Res. Lett.* **25**(14), 2465. DOI. ADS. [Thompson1998]

Verbeke, C., Pomoell, J., Poedts, S.: 2019, The evolution of coronal mass ejections in the inner heliosphere: Implementing the spheromak model with EUHFORIA. *Astron. Astrophys.* **627**, A111. DOI. ADS. [Verbeke2019]

Veronig, A.M., Brown, J.C.: 2004, A Coronal Thick-Target Interpretation of Two Hard X-Ray Loop Events. *Astrophys. J. Lett.* **603**(2), L117. DOI. ADS. [Veronig2004]

Veronig, A.M., Karlický, M., Vršnak, B., Temmer, M., Magdalenić, J., Dennis, B.R., Otruba, W., Pötzi, W.: 2006, X-ray sources and magnetic reconnection in the X3.9 flare of 2003 November 3. *Astron. Astrophys.* **446**(2), 675. DOI. ADS. [Veronig2006]

Vršnak, B.: 2008, Processes and mechanisms governing the initiation and propagation of CMEs. *Annales Geophysicae* **26**(10), 3089. DOI. ADS. [Vrsnak2008]

Warmuth, A.: 2015, Large-scale Globally Propagating Coronal Waves. *Living Reviews in Solar Physics* **12**(1), 3. DOI. ADS. [Warmuth2015]

Warmuth, A., Mann, G.: 2013, Thermal and nonthermal hard X-ray source sizes in solar flares obtained from RHESSI observations. II. Scaling relations and temporal evolution. *Astron. Astrophys.* **552**, A87. DOI. ADS. [Warmuth2013]

Warmuth, A., Mann, G.: 2016, Constraints on energy release in solar flares from RHESSI and GOES X-ray observations. II. Energetics and energy partition. *Astron. Astrophys.* **588**, A116. DOI. ADS. [Warmuth2016]

Warmuth, A., Önel, H., Mann, G., Rendtel, J., Strassmeier, K.G., Denker, C., Hurford, G.J., Krucker, S., Anderson, J., Bauer, S.-M., Bittner, W., Dionies, F., Paschke, J., Plüschke, D., Sablowski, D.P., Schuller, F., Senthamizh Pavai, V., Woche, M., Casadei, D., Kögl, S., Arnold, N.G., Gröbelbauer, H.-P., Schori, D., Wiehl, H.J., Csillaghy, A., Grimm, O., Orleanski, P., Skup, K.R., Bujwan, W., Rutkowski, K., Ber, K.: 2020, The STIX Aspect System (SAS): The Optical Aspect System of the Spectrometer/Telescope for Imaging X-Rays (STIX) on Solar Orbiter. *Solar Phys.* **295**(7), 90. DOI. ADS. [Warmuth2020]

Weiss, A.J., Möstl, C., Davies, E.E., Amerstorfer, T., Bauer, M., Hinterreiter, J., Reiss, M.A., Bailey, R.L., Horbury, T.S., O'Brien, H., Evans, V., Angelini, V., Heyner, D., Richter, I., Auster, H.-U., Magnes, W., Fischer, D., Baumjohann, W.: 2021, Multi-point analysis of coronal mass ejection flux ropes using combined data from Solar Orbiter, BepiColombo, and Wind. *Astron. Astrophys.* **656**, A13. DOI. ADS. [Weiss2021]

West, M.J., Zhukov, A.N., Dolla, L., Rodriguez, L.: 2011, Coronal Seismology Using EIT Waves: Estimation of the Coronal Magnetic Field Strength in the Quiet Sun. *Astrophys. J.* **730**(2), 122. DOI. ADS. [West2011]

Xie, H., Ofman, L., Lawrence, G.: 2004, Cone model for halo CMEs: Application to space weather forecasting. *Journal of Geophysical Research (Space Physics)* **109**(A3), A03109. DOI. ADS. [Xie2004]

Zhang, J., Dere, K.P., Howard, R.A., Kundu, M.R., White, S.M.: 2001, On the Temporal Relationship between Coronal Mass Ejections and Flares. *Astrophys. J.* **559**(1), 452. DOI. ADS. [Zhang2001]

Zhao, L.-L., Zank, G.P., He, J.S., Telloni, D., Hu, Q., Li, G., Nakanotani, M., Adhikari, L., Kilpua, E.K.J., Horbury, T.S., O'Brien, H., Evans, V., Angelini, V.: 2021, Turbulence and wave transmission at an ICME-driven shock observed by the Solar Orbiter and Wind. *Astron. Astrophys.* **656**, A3. DOI. ADS. [Zhao2021]

Zhukov, A.N.: 2007, Using CME Observations for Geomagnetic Storm Forecasting. In: Lilensten, J. (ed.) *Space Weather : Research Towards Applications in Europe 2nd European Space Weather Week (ESWW2)*, *Astrophysics and Space Science Library* **344**, 5. DOI. ADS. [Zhukov2007]

Zhukov, A.N.: 2011, EIT wave observations and modeling in the STEREO era. *Journal of Atmospheric and Solar-Terrestrial Physics* **73**(10), 1096. DOI. ADS. [Zhukov2011]

Zurbuchen, T.H., Richardson, I.G.: 2006, In-Situ Solar Wind and Magnetic Field Signatures of Interplanetary Coronal Mass Ejections. *Space Sci. Rev.* **123**(1-3), 31. DOI. ADS. [Zurbuchen2006]

Supplementary Files

This is a list of supplementary files associated with this preprint. Click to download.

- Fig14ICMEs20210422.mp4
- Fig2EUIFSI304FSI17420210422basediff.mp4
- Fig3EUIFSI17420210422.mp4
- Fig3EUIFSI30420210422.mp4